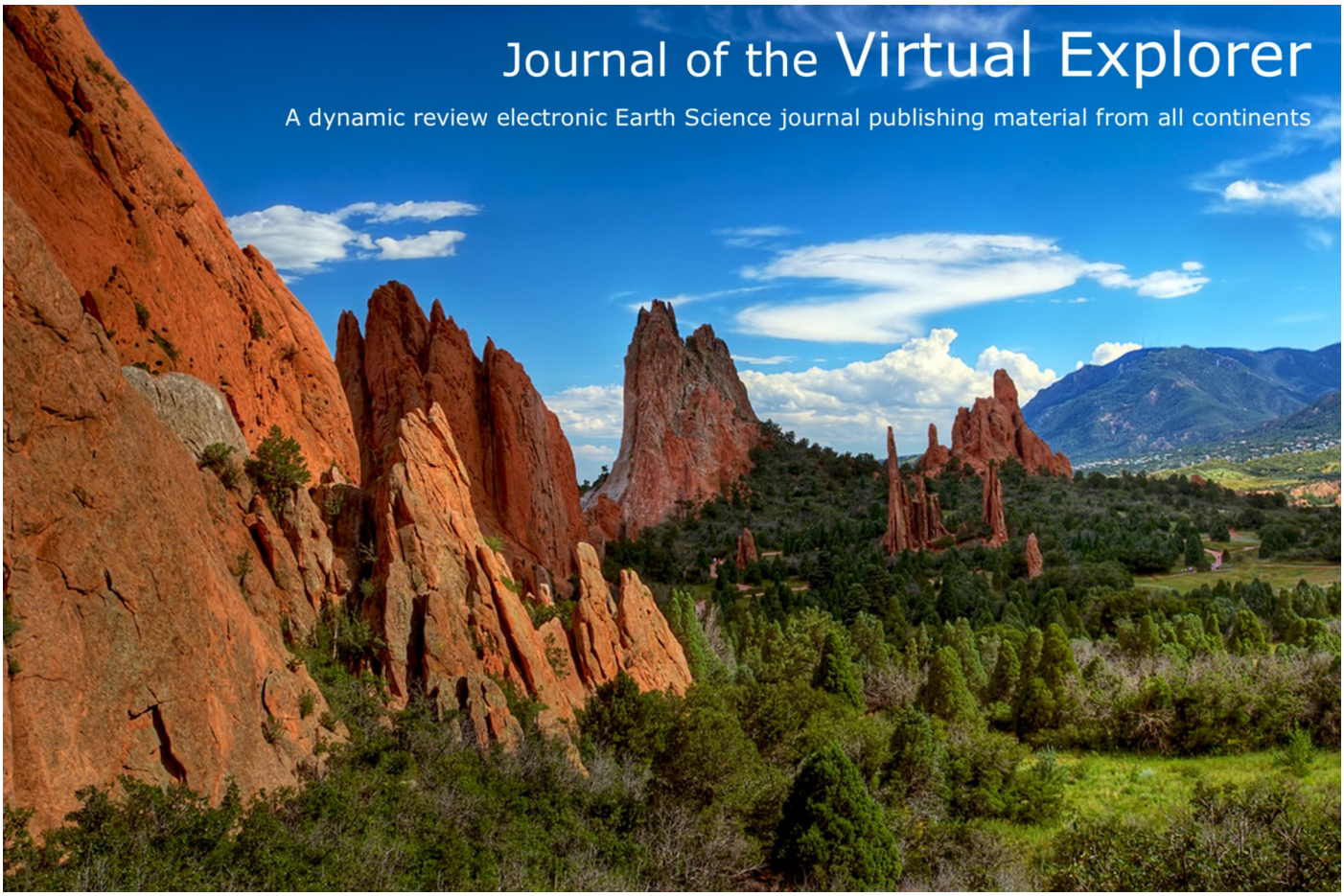

Decoding dihedral angles in melt-bearing and solidified rocks

Marian B. Holness

Journal of the Virtual Explorer, Electronic Edition, ISSN 1441-8142, volume **35**, paper 2
In: (Eds.) M.A. Forster and John D. Fitz Gerald,
The Science of Microstructure - Part I, 2010.

Journal of the Virtual Explorer, 2010
Volume 35
Paper 2
http://virtualexplorer.com.au/

Decoding dihedral angles in melt-bearing and solidified rocks

Marian B. Holness
Dept. Earth Sciences, University of Cambridge, Downing Street, Cambridge CB2 3EQ, UK.
Email: marian@esc.cam.ac.uk

Abstract: The dihedral angle is the angle subtended between two grain boundaries at a three-grain junction, or the angle between the two liquid-solid interfaces at the corner of a fluid-filled pore. In textural equilibrium the dihedral angle defines the topology, interconnectivity and amount of a liquid phase. Complete textural equilibrium (in terms of uniform grain size, constant mean curvature of grain boundaries and balancing of interfacial energies at all three- and four-grain junctions) is rare in geological materials, particularly in the crust. Local equilibrium at grain junctions (manifest as dihedral angles) is generally seen in monomineralic rocks, in high-grade metamorphic rocks and in the mantle. The distribution of true dihedral angles, as measured using a universal stage, has great potential use in interpretation of rock history. The studies of disequilibrium dihedral angles are currently at the descriptive stage, and further efforts need to be applied to deriving a quantitative understanding of the processes by which, and rates at which, they attain equilibrium.

Citation: 2010. Decoding dihedral angles in melt-bearing and solidified rocks. In: (Eds.) M.A. Forster and John D. Fitz Gerald, *Journal of the Virtual Explorer*, volume **35**, paper 2, doi: 10.3809/jvirtex.2011.00265

Introduction

Rock microstructure can preserve a wealth of information about geological history, particularly if the last recrystallisation event was insufficient to obliterate the traces of earlier episodes. Most microstructural studies interpret characteristics such as grain shape, the distribution of grain sizes and preferred orientation of grains (c.f. the comprehensive reviews by Vernon (2004) and Higgins (2006)). Other parameters of interest are the shape of grain boundaries and interfaces (e.g. Kruhl, 2001; Kruhl and Peternell, 2002). A comparatively neglected microstructural parameter is the dihedral angle, that angle subtended between two grain boundaries or interfaces (Smith, 1948; 1964). Although dihedral angles in rocks have been studied for decades, due to their importance in determining the equilibrium distribution of a liquid phase (Smith, 1964; Wray, 1976; Bulau *et al.*, 1979; von Bargen and Waff, 1986), it has only recently become apparent that in many rocks the population of dihedral angles is far from equilibrium (e.g. Sawyer, 1999; Kruhl and Peternell, 2002; Holness *et al.*, 2005a), and that this departure from equilibrium provides a window into rock history. Dihedral angles are particularly useful in that they are relatively straightforward to quantify and tend to undergo the earliest changes during recrystallisation (Voll, 1960): they are thus highly sensitive to changes in physical conditions (particularly temperature). The disequilibrium angle population is a useful record of processes such as recrystallisation, solidification and reaction and is used as a qualitative indicator of the thermal history. Here I review the current level of understanding of both equilibrium and disequilibrium dihedral angle populations, outline how they may be interpreted, and provide pointers for further research. The focus is on melt-bearing and solidified rocks, because the rarity of preserved volatile-filled pores in metamorphic and igneous rocks reduces the usefulness of volatile-solid dihedral angle data.

Textural Equilibrium

Textural equilibrium is reached when a material has minimized the energies bound up in interfaces and within individual grains (Figure 1a). This state can only be attained once the material is defect-free and in chemical and mechanical equilibrium. The free energy of an interface in an isotropic system (i.e. the energy of the interface is constant regardless of its orientation relative to any crystal lattice) is typically of the order 1 Jm^{-2} (Sutton and Baluffi, 1996), and is a function of its curvature (Harker and Parker, 1945). The chemical activity of a system with curved interfaces is higher than that in a system with planar interfaces (Bulau *et al.*, 1979). Because of this, all interfaces must have the same mean radius of curvature. This can only be attained in isotropic systems if grain-size is uniform.

For anisotropic substances, certain orientations of the surface have a lower energy than others and so it is possible to reach a minimum energy state with a mixture of planar and curved surfaces (Herring, 1951a; Waff and Faul, 1992). This is particularly important for geological materials such as amphiboles (Figure 1b) and sheet silicates, although grain boundaries in even relatively isotropic quartz have significant planar regions (Kruhl, 2001; Kruhl and Peternell, 2002; Leibl *et al.*, 2007).

A further constraint is that the energies of the interfaces at three- and four-grain junctions must be in mechanical equilibrium, satisfying:

$$\sum_{i=1}^{3}\left(\gamma_i t_i + \frac{\partial \gamma_i}{\partial t_i}\right) = 0$$

where γ_1, γ_2, γ_3 are the three interfacial energies, $\mathbf{t}_i$ is the vector in the plane of the i^{th} surface, normal to the line of intersection of the surfaces and pointing away from this line, and $\partial\gamma_i/\partial\mathbf{t}_i$ is a vector perpendicular to $\mathbf{t}_i$ and to the line of intersection (Herring, 1951b). The tangential component of this equation acts to minimize the surface area, while the normal component rotates the interface towards an orientation with a lower interfacial area.

For an isotropic polycrystalline material, in which the interfacial energy is constant regardless of the orientation of the interface, the normal term vanishes: three-grain junctions therefore meet at 120˚, while the four three-grain junctions where four grains meet are 109˚28’ apart. For poly-phase junctions the angle between two interphase boundaries is known as the dihedral angle (Smith, 1948; 1964), and for two-phase junctions in isotropic systems the simplified form of this equation becomes:

$$\gamma_{11} = 2\gamma_{12}\cos\left(\frac{\theta}{2}\right)$$

where γ_{11} is the energy of the boundary between two grains of phase 1, γ_{12} is the energy of the inter-phase boundary, and θ is the dihedral angle (Figure 1c).

Figure 1. Texturally equilibrated microstructures

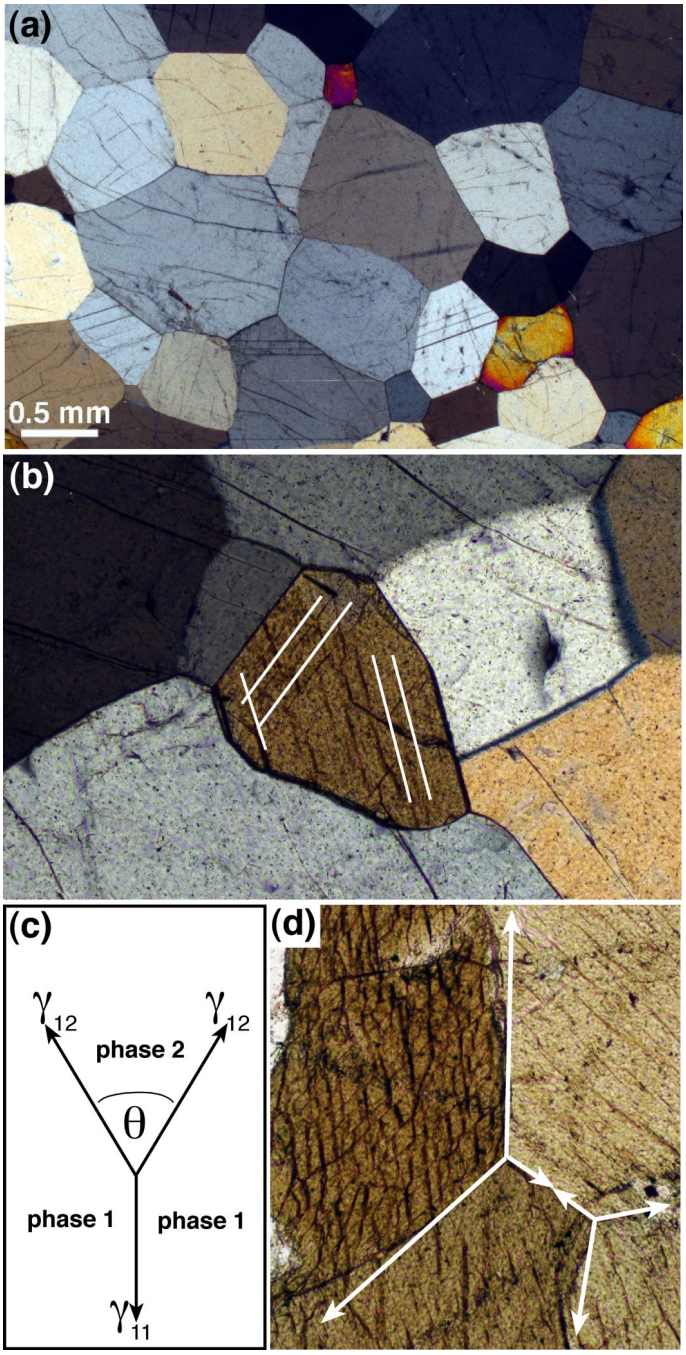

(a) epidote-hornblende quartzite (sample 87974 from the Cambridge Harker Collection) showing microstructural evidence for a close approach to textural equiibrium. (b) detail of the rock shown in (a), showing an amphibole grain surrounded by quartz. The shape of the amphibole is dominated by {110} faces (parallel to the cleavage which is picked out by white lines). These faces are particularly low energy and so form part of the equilibrated microstructure. (c) The dihedral angle, θ, is formed by balancing of the interfacial energies at three-grain junctions. (d) Texturally equilibrated amphibolite (Aboyne, Deeside, sample 102032 from the Cambridge Harker Collection). The white lines show the tangents to the curved grain boundaries. The dihedral angles at the three-grain junctions should be measured between these tangents.

However, all geological materials have some form of anisotropy (e.g. Kretz, 1966; Schafer and Foley, 2002) and so there is no single value of the equilibrium dihedral angle (Herring, 1951b; Laporte and Watson, 1995; Laporte and Provost, 2000; Kruhl, 2001): the angle varies according to the relative orientation of the grains at the junction with a greater spread of possible angles for the more anisotropic minerals (e.g. Vernon, 1968; Laporte and Provost, 2000). The least anisotropic minerals (i.e. those with a tighter spread of equilibrium angles) include quartz, calcite and feldspars, while the most anisotropic include micas and amphiboles (Laporte and Watson, 1995).

In texturally equilibrated melt-bearing rocks, the melt-solid-solid dihedral angle has significant consequences for rock physical properties via its underlying control on melt topology (Takei, 2000; Yoshino *et al.*, 2005; Hier-Majumder *et al.*, 2006; Price *et al.*, 2006; Parsons *et al.*, 2008; Pervukhina and Kuwahara 2008). In isotropic systems in which the liquid-solid-solid dihedral angle falls below a critical value of 60˚ the liquid phase remains interconnected along a series of channels on three-grain junctions down to vanishingly low porosities. However the facetted pore walls present in equilibrated anisotropic materials mean that this connectivity is broken when the porosity falls below a few vol. % (Minarik and Watson, 1995; Laporte and Watson, 1995; Yoshino *et al.*, 2002; Cheadle *et al.*, 2004; Yoshino *et al.*, 2006; Price *et al.*, 2006). In open systems the porosity is also a function of the dihedral angle: melt is either infiltrated or expelled as the system attempts to attain the value of porosity at which the interfacial energy budget is minimized. This minimum energy porosity reaches a maximum value of ~ 20 vol.% for angles of 60˚, declining to zero for angles above 60˚ (Park and Yoon, 1985; Laporte and Watson, 1995).

The last stage of textural equilibration (termed "textural coarsening" by Higgins (2010)) involves grain growth. This has the effect of reducing the connectivity of any melt phase with a dihedral angle greater than 60˚

due to what is called “pinging off” of melt-filled channels on three-grain junctions (Bagdassarov *et al.*, 2009). Because the end point of energy minimization is when the material comprises infinitely large defect-free grains, true textural equilibrium is only ever approached and never reached.

How To Measure Dihedral Angles

Early work on dihedral angles was done primarily on metals (Smith, 1964) and sulfides (Stanton and Gorman, 1968): these are opaque and so the first measurement techniques developed were appropriate for polished sections. The apparent dihedral angle measured on a 2-D section through a polycrystalline material depends on the relative orientation of the grain boundaries and the sample surface, being either higher or lower than the true value. Smith (1948) demonstrated that in a sample with randomly oriented grain boundaries and a single value of true dihedral angle the mode of a theoretical distribution of apparent angles has the same value as the true dihedral angle. However, the mode is a difficult parameter to constrain accurately as it requires a large population of measured angles: ~200 measurements are required to obtain a value for the mode which lies within 5˚ of the true angle (Harker and Parker, 1945). An easier measure to constrain is the median, and the median of a theoretical distribution of apparent angles is always within 1˚ of the true value. Riegger and Van Vlack (1960) showed that only ~25 measurements to achieve a similar degree of accuracy to Harker and Parker (1945).

Many studies of geological materials rely on observation of polished opaque fragments (e.g. experimental run charges) and therefore are reliant on interpretation of apparent angles. However, as first pointed out by Stickels and Hücke (1964), many observed distributions depart from those predicted for equilibrated single-valued aggregates. The departure may be due to errors in measurement or the effects of preferred alignment of non-equant grains via a variation of apparent particle size. For most geological materials it is likely that the bulk of the departure is caused by the presence of a range of true angles, due either to incomplete textural equilibration or crystalline anisotropy (Laporte and Provost, 2000; Leibl *et al.*, 2007). Extracting the range of true angles from a set of measurements from a 2-D section is not straightforward (Riegger and Van Vlack, 1960; Stickels and Hücke, 1964; Jurewicz and Jurewicz, 1986; Vernon, 1997; Laporte and Provost, 2000).

As pointed out by Vernon (1997) the interpretational problems associated with measurements of apparent angles can be avoided completely for translucent samples. The range of true angles in a petrological thin-section can be constrained directly using a universal stage mounted on an optical microscope (see the accessible review by Kile (2009)). This instrument permits the rotation of grain boundaries into alignment with the line of sight, thus permitting the measurement of the true dihedral angle. True angles can be also measured using transmission electron microscopy (Cmíral *et al.*, 1998). Early work on dihedral angles in geological materials used the universal stage (e.g. Voll, 1960; Vernon, 1968) but it subsequently fell into general disuse, perhaps because it is no longer introduced to undergraduates, having become obsolete for many of its original purposes.

Use of the universal stage requires a petrological microscope with a sufficiently large distance between the objectives and the planar rotating stage (most microscopes dating from 1970 or earlier will suffice) together with a long working distance objective (such as those used for heating stages for fluid inclusion work). The minimum magnification for dihedral angle work is about x30 (I use the Leitz UM32 objective; no longer in production but obtainable from collectors and traders in microscope equipment).

Universal stage measurement of dihedral angles can be learnt quickly. The angle to be measured (generally in plane–polarised light) is located at the cross-hairs and the section is rotated (using trial and error) until all three grain boundaries in the immediate vicinity of the junction are sharply defined (and thus oriented parallel to the direction of view). It is important that the angle is measured right at the junction itself, and for curved boundaries it is necessary to measure the angle between the tangents to the boundary (Figure 1d) – this takes practice but is otherwise straightforward. A further consideration is that many grain boundaries may be facetted in the immediate vicinity of the junction and care must be taken to measure the angle at the junction itself (Kruhl, 2001). The analyzer can be used to provide a check that the boundaries are truly parallel to the direction of view: inclined boundaries in relatively highly birefringent materials will have variable birefringence or interference fringes. Measurement of the angle is then a matter of using the gradations

on the rotating stage to read off the angle between the two boundaries of interest.

Measurement errors

There are several possible sources of error in determining the dihedral angle population. The first, relevant to measurement of both apparent angles in 2-D and true angles in 3-D, is a simple measurement bias, with undue emphasis given to angles in a particular size range. The universal stage provides a useful check on this possibility, since the observer does not generally have much idea how large the angle is until some effort has been expended in orienting the junction correctly. However, a major source of possible sampling error for very large angles arises when the A-A grain boundary (for the angle at A-A-B junctions) is not clearly visible. Such high angles may be easily overlooked as they will appear to be part of a single A-B junction: this problem typically occurs when measuring augite-plagioclase-plagioclase angles in plane polarized light. A simple way to avoid this is to insert the analyzer when searching for angles to measure, making it obvious where the plagioclase-plagioclase grain boundaries meet a grain of another phase.

Another source of error is that associated with an individual measurement. Each researcher needs to determine his or her own margin of error, perhaps by measuring the same angle many times. It is typically of the order of a few degrees (e.g. Gleason *et al.*, 1999).

The final source of error is more complex. Because we don't know the distribution function of the underlying (parent) population that is being sampled, it is not straightforward to work out the error on the median or standard deviation of a population of measured angles. Stickels and Hücke (1964) developed a non-parametric method, based on the assumption that the population has a continuous distribution function of some unknown form, to establish a confidence interval for the median angle of a population independent of its actual distribution. They present the confidence intervals as a function of different sample sizes (reproduced here as Table 1). For example, for a sample of 100 measurements, listed in order of their magnitude, there is only one chance in twenty that the median value will not lie between the values of the 40th and 60th measurements.

Table 1. Confidence interval for population median for samples of various sizes

Sample size	**90% confidence interval**	**95% confidence interval**	**99% confidence interval**
25	9 to 17	8 to 18	6 to 20
50	19 to 32	18 to 33	16 to 35
75	30 to 45	29 to 46	26 to 50
100	42 to 58	40 to 60	37 to 63
250	112 to 138	110 to 140	105 to 145
500	232 to 268	228 to 272	221 to 279
1000	474 to 526	469 to 531	459 to 541

The confidence interval for the median of a population sampled by varying numbers of individual measurements. From Stickels and Hücke (1964).

To illustrate the errors associated with dihedral angle measurements a suite was chosen of nine samples with very different dihedral angle populations (Figure 2a and Table 2, with the full data set provided in Table 3.) Click to download Table 3. For each rock, a large number of measurements were made of the true dihedral angle. Several thin sections were used for rocks in which suitable three-grain junctions were rare. The standard deviations of the parent populations vary from 10˚ to 25˚, with median values between 60˚ and 114˚. There is a negative correlation between the median and standard deviation (c.f. Holness *et al.*, 2005a). The error on the median was determined using the method of Stickels and Hücke (1964), and the 95% confidence interval is presented in Table 1. The error associated with each median value increases with the spread of the populations.

Figure 2. An analysis of errors associated with the standard deviation and the median dihedral angle

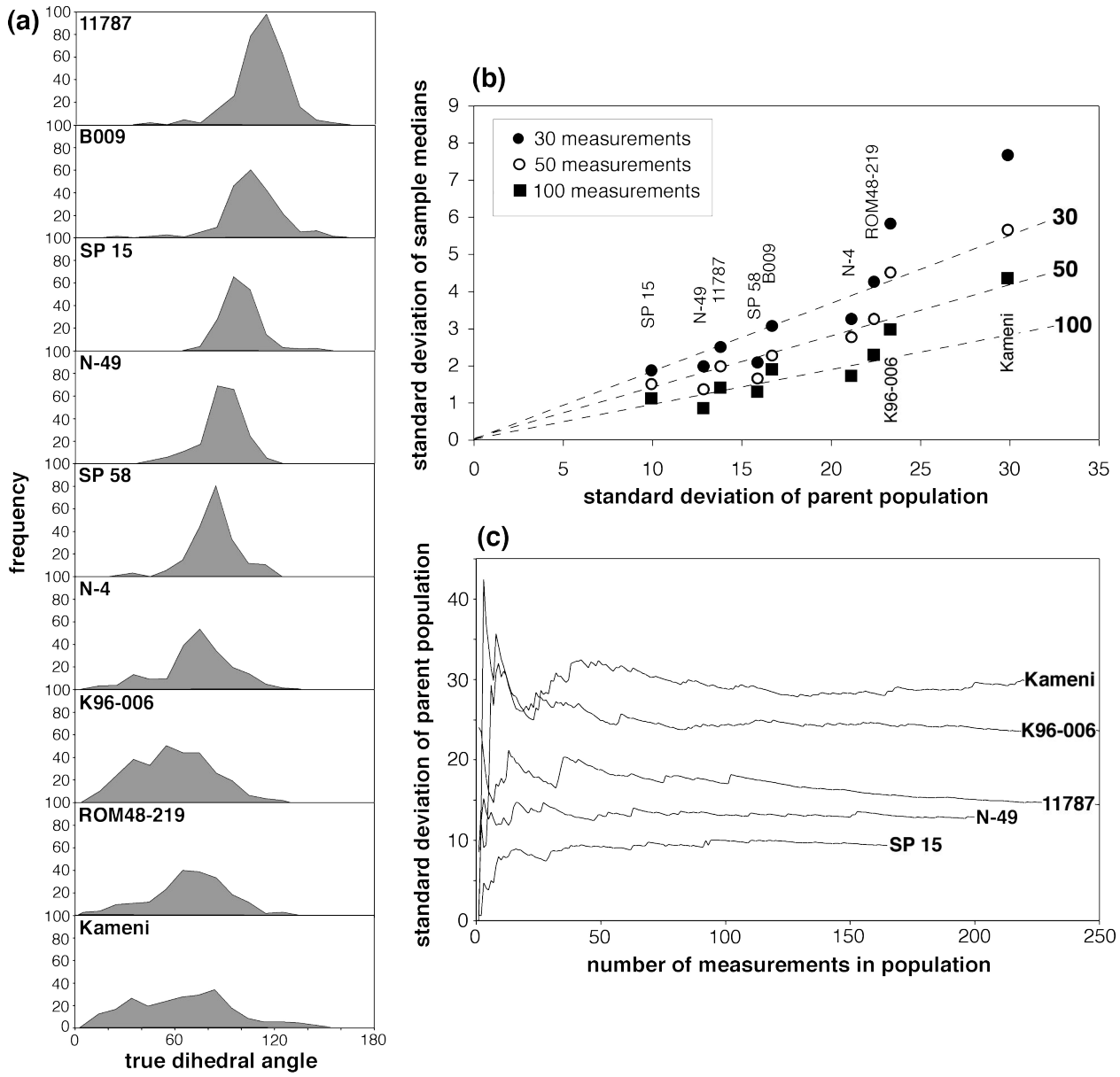

(a) frequency plots of true dihedral angles measured in the series of rocks detailed in Table 2. (b) The standard deviation of the median value of a small population taken from the larger populations shown in (a), plotted as a function of the standard deviation of the parent population. The dashed lines are the standard deviations of the median calculated assuming the parent population has a normal distribution labeled according to the number of measurements taken from the parent. (c) The standard deviation of a population as a function of the increasing number of measurements for a representative subset of the nine rocks shown in (a) and (b).

Table 2. Errors associated with dihedral angle measurements

Sample	Phases	n	median	s.d.	Description	Locality	Reference
SP 15	augite-plag-plag	166	99° ± 1°	10.0°	gabbro	Skaergaard Marginal Border Series	Kramer Ø
N-49	augite-plag-plag	201	90° ± 1°	12.9°	gabbro	Rum Eastern Layered Intrusion, Unit 10 allivalite	Sides (2008)
11787	augite-plag-plag	300	114° ± 1°	13.8°	granulite	Peruga, South India (Harker Collection	Cambridge)
SP 58	augite-plag-plag	200	84° ± 1°	15.9°	gabbro	Skaergaard Marginal Border Series	Kramer Ø
B009	augite-plag-plag	200	106° ± 2°	16.7°	gabbro	Rum Eastern Layered Intrusion, Unit 9 allivalite	Holness *et al.* (2007b)
N-4	augite-plag-plag	200	74° ± 2°	21.2°	troctolite	Rum Eastern Layered Intrusion, Unit 10 allivalite	Sides (2008)
ROM48-219	augite-plag-plag	200	71° ± 3°	22.4°	dolerite	Traigh Bhan na Sgurra sill, Ross of Mull.	Holness & Humphreys (2003)
K96-006	glass-amph-amph	300	60° ± 3°	23.3°	enclave	Kula Volcanic Province, Western Turkey	Holness & Bunbury (2006)
Kameni	glass-plag-plag	230	66° ± 5°	29.9°	enclave	Kameni Islands, Santorini, Greece	Martin *et al.* (2006)
70424 A	augite-plag-plag	100	98° ± 1.5°	8.9°	gabbro	Stillwater Intrusion, Montana. ⊥ foliation	From the Harker Collection
70424 B	augite-plag-plag	100	99° ± 2°	9.1°	gabbro	Stillwater Intrusion, Montana. ⊥ foliation	
70424 C	augite-plag-plag	97	98° ± 1.5°	9.0°	gabbro	Stillwater Intrusion, Montana. // foliation	

The Virtual Explorer
http://virtualexplorer.com.au/
Journal of the Virtual Explorer, 2010
Volume 35
Paper 2

Using these large measurement populations we can simulate the process of taking a limited sample population from an unknown parent population and approximate the effects of sample size. 200 random sample populations of 30, 50 and 100 angles were chosen from these parent populations (i.e. 600 randomly chosen sample populations for each rock). The median values for each of the 600 randomly chosen sample populations vary about the median of the parent population. The standard deviation of this variation provides a measure of the accuracy of the median values for the sample populations and, as expected, the median values show less variability within the larger sample populations. The standard deviation, 1σ, of these median values is shown as a function of sample size and the standard deviation of the parent population in Figure 2b. For comparison the standard deviation is also shown of median values picked at random from an unknown parent population with a *normal* distribution. It is interesting that the data from natural samples scatter about that expected for a normal distribution for relatively tightly distributed parent populations, suggesting that the natural sample populations are generally rather close to normal.

For rocks in which the texture is at, or close to, textural equilibrium (for which the standard deviation is generally <15˚, Holness *et al.*, 2005a), the true value of the median is likely to be closely approached (i.e. a 95% confidence interval of ±2˚) for a sample of 100 measurements. A similarly sized population for a sample far from equilibrium (with a standard deviation > 20˚) is likely only to be correct within ±6˚.

This sensitivity of the error to the distribution of the underlying parent population means that it is helpful to have an idea of the spread of true angles. Figure 2c shows the variation of the standard deviation as a function of the number of individual measurements for a selection of samples of varying angle distributions. Typically the standard deviation tends towards an asymptote after 50 - 100 measurements.

While one should conclude from this analysis that the ideal number of measurements is ≥100 angles, for large-scale studies 100 angles per sample involves a significant time investment. This can be avoided in some instances, particularly if it is known that all the samples have a similar genesis. As an example, members of a suite of cumulates from a single layered intrusion are likely to have had similar solidification histories. If a small subset of these are examined in detail to determine the general pattern of the angle distribution functions, it might be justifiable to base one's conclusions on comparisons of the median value and reduce the number of angle measurements in the rest of the samples to 30 – 50.

Reporting results

The earliest work on dihedral angles (e.g. Harker and Parker, 1945) was based on the idea that all dihedral angles in a material are the same. If this is the case a true and complete measure of the angle population is provided by the mode (*ibid.*) or median (Riegger and Van Vlack, 1960) of the population of apparent angles. However, equilibrated poly-crystals containing anisotropic minerals will contain a range of dihedral angles and it is not clear what meaning can be attached to either the mode or the median. Stickels and Hücke (1964) recognized this and suggested the material can be characterized by an "effective dihedral angle", equivalent to the median value of the apparent angle population. Most of the published work on true, 3-D, dihedral angles is based on comparisons of median values (e.g. Holness *et al.*, 2005a; 2007a), with its attendant advantage of not needing many individual measurements. Other studies report the mode of (larger) populations (Vernon, 1968; Lusk *et al.*, 2002) or present cumulative frequency plots (Kruhl, 2001; Leibl *et al.*, 2007).

However, the distribution function of the true dihedral angles potentially holds important information, and this is lost if only the median is presented. The standard deviation gives an idea of the spread, but a true picture of the angle population can only be given if it is presented as a frequency plot. This is particularly important in strongly poly-modal samples in which the median value will fluctuate depending on the balance of the two dihedral angle populations; for such samples the results should be presented as a frequency plot (e.g. Holness and Sawyer, 2008).

Dihedral Angles in Texturally Equilibrated Rocks

Solid materials

A summary of the published values for solid-solid-solid dihedral angles of geological relevance is presented in Table 4, with an indication of whether the results are the medians of populations of apparent angles measured

on 2-D sections or whether they pertain to true 3-D values. Angle populations in single-phase materials have a median value of 120˚ (the only possible result when all three angles at each triple junction are included), with a range dependent on the extent of anisotropy of grain boundary energy (e.g. Kruhl, 2001; Leibl *et al.*, 2007). For two-phase junctions, angle distributions tend to have a standard deviation in the region of 10-15˚.

Table 4. Solid-solid-solid equilibrium dihedral angles of geological relevance

Phases	**Median dihedral angle**	**Range of true angles**	**Reference**
Sphalerite-galena-galena	134°		Stanton (1964)
Sphalerite-galena-galena	111 – 128°		Lusk *et al.* (2002)
Chalcopyrite-sphalerite-sphalerite	130°		Stanton (1964)
Pyrrohtite-sphalerite-sphalerite	102 – 114°		Lusk *et al.* (2002)
Galena-sphalerite-sphalerite	133°		Stanton (1964)
Galena-sphalerite-sphalerite	27 – 111°		Lusk *et al.* (2002)
Quartz-orthoclase-orthoclase		52 – 149°	Vernon (1968)
Quartz-plag-plag		79 – 139°	Vernon (1968)
Quartz-plag-plag	106°		Hiraga *et al.* (2002)
Quartz-garnet-garnet		43 – 138°	Vernon (1968)
Quartz-calcite-calcite		68 – 146°	Vernon (1968)
Quartz-apatite-apatite		35 – 107°	Vernon (1968)
Plag- quartz-quartz		71 – 158°	Vernon (1968)
Plag-quartz-quartz	117°		Hiraga *et al.* (2002)
Plag-hornblende-hornblende		27 – 149°	Vernon (1968)
Plag-hornblende-hornblende		55 – 163°	Vernon (1970)
Plag-augite-augite		57 – 170°	Vernon (1968)
Plag-augite-augite		30 – 159°	Vernon (1970)
Orthoclase-garnet-garnet		38 – 132°	Vernon (1968)
Garnet-quartz-quartz		90 – 180°	Vernon (1968)
Garnet-orthoclase-orthoclase		94 – 165°	Vernon (1968)
Hornblende-augite-augite		83 – 180°	Vernon (1968)
Hornblende-plag-plag		46 – 180°	Vernon (1968)
Hornblende-plag-plag		62 – 162°	Vernon (1970)
Augite-plag-plag		72 – 150°	Vernon (1968)
Augite-plag-plag		52 – 155°	Vernon (1970)
Augite-olivine-olivine	79°		Toramaru & Fujii (1986)
Augite-orthopyroxene-orthpyroxene	86°		Toramaru & Fujii (1986)
Orthopyroxene-olivine-olivine	106 – 114°		Fujii *et al.* (1986)

Phases	Median dihedral angle	Range of true angles	Reference
Orthopyroxene-olivine-olivine	91°		Toramaru & Fujii (1986)
Orthopyroxene-augite-augite	113.5°		Toramaru & Fujii (1986)
Olivine-orthopyroxene-orthopyroxene	119 – 122°		Fujii *et al.* (1986)
Olivine-orthopyroxene-orthopyroxene	117°		Toramaru & Fujii (1986)
Olivine-augite-augite	129°		Toramaru & Fujii (1986)
Ilmenite-orthoclase-orthoclase		92 – 162°	Vernon (1968)
Calcite-quartz-quartz		98 – 152°	Vernon (1968)
Apatite-quartz-quartz		87 – 180°	

The sensitivity of equilibrium angles to pressure and temperature has been little studied. The population of true equilibrium dihedral angles in quartz aggregates (the quartz-quartz-quartz angle) is not sensitive to temperature (Kruhl, 2001), whereas the median of equilibrium two-phase (apparent) dihedral angles in sulphides (e.g. at sphalerite-galena-galena junctions) decreases significantly with increasing temperature, with potential use as a geothermometer (Stanton and Gorman, 1968; Lusk *et al.* 2002).

Melt-bearing materials

A summary of the published values for melt-solid-solid dihedral angles of relevance to melt-bearing rocks is given in Table 5. Most of the published measurements have been made on 2-D sections; the reported values for these studies are the medians of the measured population. Only two studies to date have reported measurements of true 3-D angles (Cmíral *et al.* 1998, Holness, 2006). Typical frequency distributions of the true 3-D angles are shown in Figure 3.

Table 5. Melt-solid-solid equilibrium dihedral angles of geological relevance

solid	melt	Range of median angles	Median of true 3-D angles	source
quartz	Dry Silicic	60°		Jurewicz & Watson (1984)
quartz	Dry silicic	59°		Jurewicz & Watson (1985)
quartz	Hydrous silicic melt	12 – 18°		Laporte (1994)
quartz	Hydrous silicic melt	34 – 58°		Holness (1995)
quartz	rhyolite		19°, s.d. 9.7°	Holness (2006)
feldspar	Dry silicic	44°		Jurewicz & Watson (1985)
plagioclase	Anorthositic melt	45°		Longhi & Jurewicz (1995)
feldspar	silicic	41 – 54°		Gleason *et al.* (1999)

solid	**melt**	**Range of median angles**	**Median of true 3-D angles**	**source**
feldspar	silicic		28.5°, s.d. 12.2°	Laporte & Provost (2000)
plagioclase	basalt		26°, s.d. 11.6°	Holness (2006)
plagioclase	rhyolite		24°, s.d. 11.5°	Holness (2006)
plagioclase	Inninmorite (64 wt.% SiO_2)		23°, s.d. 10.2°	Holness (2006)
leucite	tephrite		20°, s.d. 10.9°	Holness (2006)
silicate	Fe-Ni-S alloy	99 – 125°		Shannon & Agee (1996)
perovskite	Fe melt	51 – 94°		Takafujii *et al.* (2004)
perovskite	Fe-O-S liquid	79 – 102°		Terasaki *et al.* (2007)
perovskite	Fe-Si alloy	130 – 140°		Mann *et al.* (2008)
olivine	Fe-Ni-S alloy	60 – 93°		Minarik *et al.* (1996)
olivine	Fe-Ni-S-O melt	96 – 106°		Holzheid *et al.* (2000)
olivine	Fe-S alloy	66 – 106°		Terasaki *et al.* (2005)
olivine	Fe-O-S alloy	54 – 98°		Terasaki *et al.* (2008)
olivine	basalt	47°		Waff & Bulau (1979)
olivine	basalt	41 – 47°		Fujii *et al.* (1986)
olivine	basalt	49°		Toramaru & Fujii (1986)
olivine	basalt	0 – 10°		Cmíral *et al.* (1998)
olivine	basalt		29°, s.d. 12.7°	Holness (2006)
olivine	"silicate melt" (basalt°)	0 – 45°		Yoshino *et al.* (2009)
olivine	picrite		29°, s.d. 9.0°	Holness (2006)
olivine	carbonatite	28°		Hunter & McKenzie (1989)
olivine	carbonatite	23 – 36°		Watson *et al.* (1990)
olivine	carbonatite	25 – 30°		Minarik & Watson (1995)
olivine	Si-rich mantle melt	50°		Maumus *et al.* (2004)
olivine	phonolite		29°, s.d. 11.9°	Holness (2006)
olivine	komatiite	32 – 33°		Jurewicz & Jurewicz (1986)
olivine	komatiite	29 – 33°		Walker *et al.* (1988)
hornblende	Silicic melt	25°		Laporte & Watson (1995)

solid	melt	Range of median angles	Median of true 3-D angles	source
hornblende	Granitic melt	53 – 58°		Lupulescu & Watson (1999)
hornblende	Tonalitic melt	46 – 48°		Lupulescu & Watson (1999)
biotite	Silicic melt	23 - 39		Laporte & Watson (1995
augite	basalt	98°		Toramaru & Fujii (1986)
diopside	Diopside-anorthite melt	33 – 60°		Ikeda *et al.* (2002)
augite	Inninmorite (64 wt.% SiO_2)		38°, s.d. 13.4°	Holness (2006)
augite	phonolite		37°, s.d. 14.8°	Holness (2006)
augite	basalt		37.5°, s.d. 13.0°	Holness (2006)
orthopyroxene	basalt	52 – 70°		Fujii *et al.* (1986)
orthopyroxene	basalt	76°		Toramaru & Fujii (1986)
orthopyroxene	basalt	20 – 40°		Von Bargen & Waff (1988)
chromite	Sulphide liquid	41 – 53°		Brenan & Rose (2002)

Figure 3. Texturally equilibrated melt-solid-solid dihedral angles

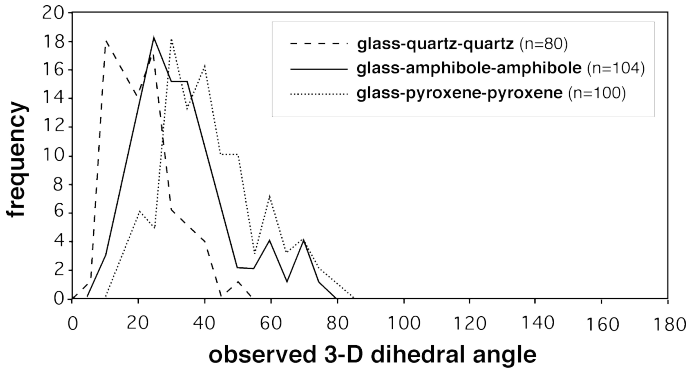

Frequency distributions of true dihedral angles measured for texturally equilibrated natural examples of rapidly quenched melt-bearing systems. From Holness (2006).

The variation of the liquid-solid-solid equilibrium dihedral angle with pressure, temperature and fluid composition is controlled by the layer of adsorbed species on the interfaces (Holness, 1993; Brenan and Rose, 2002; Takei and Shimizu, 2003). In general, the higher the extent of surface activity the more sensitive is the equilibrium angle to changes in pressure and temperature (Holness, 1993; Holness and Graham, 1995).

If the liquid has a similar composition and structure to the solid then the energy of the liquid-solid interface, and thus the dihedral angle, is low. The smallest angles are generally found in single component systems such as ice-water (Walford and Nye, 1991; although see Mader (1992)) or systems with very high solubility of the solid phase (e.g. sucrose-H_2O, Pharr and Ashby, 1983; NaCl-H_2O ice, Spetzler and Anderson, 1968; olivine-H_2O at high pressure, Yoshino et al, 2007). In simple binaries, the dihedral angle is a function of temperature (and thus liquid composition), with the lowest angles when the liquid composition is closest to that of the solid phase (Takei, 2000; Ikeda *et al.*, 2002; Takei and Shimizu, 2003).

Conversely, the highest angles occur where the solid and liquid have the most disparate compositions and structures. Examples of the latter include argon-calcite, argon-quartz, CO_2-quartz (Holness 1993), metal-olivine (see list of references in Table 5). Fe-S liquids in silicate matrices also have generally high dihedral angles (e.g. Ballhaus and Ellis, 1996; Minarik *et al.*, 1996; Gaetani and Grove, 1999; Terasaki *et al.*, 2007; again see Table 5 for a more comprehensive list) although these are sensitive to changes in oxygen fugacity and pressure (Gaetani

and Grove, 1999; Rose and Brenan, 2001; Takafuji *et al.*, 2004; Terasaki *et al.* 2008).

Dihedral Angles in Non-Equilibrated Rocks

The effect of deformation on dihedral angles

While the distribution of liquid under hydrostatic conditions is controlled by the equilibrium dihedral angle (with complete interconnectivity of liquid in channels along 3-grain junctions for angles below 60˚), melt films on grain boundaries may develop during ductile deformation (Borsch and Green, 1990; Jin *et al.* 1994; Bai *et al.*, 1997; Hier-Majumder and Kohlstedt, 2006). These melt films are only stable under static conditions if the dihedral angle is zero, and this is not the case for geological materials. Thus the *effective* dihedral angle is zero during the deformation. Once deformation has ceased, the melt will regain its equilibrium geometry (c.f. Parsons *et al.*, 2008).

Jin *et al.* (1994) and Bai *et al.* (1997) found this wetting effect only with recrystallisation-accompanied dislocation creep, suggesting that the deformation mechanism is important in determining the melt geometry. However, this is not universal: Gleason *et al.* (1999) found that melt-solid-solid dihedral angles in experimentally deformed quartzo-feldspathic aggregates were similar to those present during hydrostatic annealing. Neither Dimanov *et al.* (1998) nor Hirth and Kohlstedt (1995a, b) found melt films, in deformed synthetic labradorite and olivine respectively, regardless of deformation mechanism. The controls on melt film formation are as yet not understood.

Deformation may also affect the topology of the fluid phase if overpressure leads to hydrofracture. Grain boundaries can be temporarily wetted (i.e. an effective dihedral angle of zero) but these continuous films neck down into isolated pores once deformation has ceased (e.g. Kostenko *et al.*, 2002).

Dihedral angles during prograde events

Microstructures formed during reaction (or deformation) are likely to have been overprinted during uplift. The most obvious example of this is in rocks that have undergone partial melting during regional metamorphism: such rocks (migmatites) are now fully solidified with loss of the original melt-bearing microstructures during crystallization (Sawyer, 1999). We can infer what they might have looked like using experiments (Mehnert *et al.*, 1973) or examples of rapidly-cooled partially melted rocks (e.g. Cesare *et al.* 1997; Holness *et al.*, 2005b) but much of the following is based on inference from fully solidified rocks.

Melt-solid-solid dihedral angles

Where the reaction overstep is significant, the driving force for chemical equilibration will be larger than that driving textural equilibration: melt distributions and the melt-solid-solid dihedral angle population will therefore be controlled by reaction kinetics rather than interfacial energies. It is only when the overstep is small that the rates of reaction are sufficiently slow for the texture to remain in equilibrium. This is illustrated by a series of heating and cooling experiments in the system diopside-anorthite, in which significant hysteresis was observed in the diopside-melt dihedral angle (Ikeda *et al.* 2002). Under isothermal conditions the dihedral angle decreases with temperature (due to changes in the melt composition). However, during heating the angle decreases below equilibrium values, and during cooling the angle increases beyond the equilibrium value. The extent of departure from the equilibrium values increases as the rate of temperature change increases. This hysteresis is explained by the development of compositional boundary layers around the diopside grains that are either enriched (during heating) or depleted (during cooling) in the diopside component thus leading to angles either lower or higher than those expected for equilibrium. Ikeda *et al.* (2002) point out that this hypothesis necessitates significant mass transport within the boundary layer either towards or away from the melt-solid-solid junction, although they provide no information about changes in curvature of the interfacial boundaries near the junctions. If correct it may have important implications for melt-bearing systems: this type of problem warrants further investigation.

In the case of a previously melt-free rock such as a migmatite, experimental studies and observation of rapidly quenched pyrometamorphic rocks show that in the earliest stages of melting melting on grain boundaries between the reacting phases forms a generally parallel-sided liquid film (Mehnert *et al.*, 1973; Holness *et al.*, 2005b). Grain boundaries intersect the melt film at ~ 180˚ (Figure 4a). Some melting reactions involve three phases and in this case the melt film may propagate along grain

boundaries with a correspondingly small angle at the tip (Figure 4b; Holness and Sawyer, 2008).

Figure 4. Melt-solid-solid dihedral angles in melting rocks

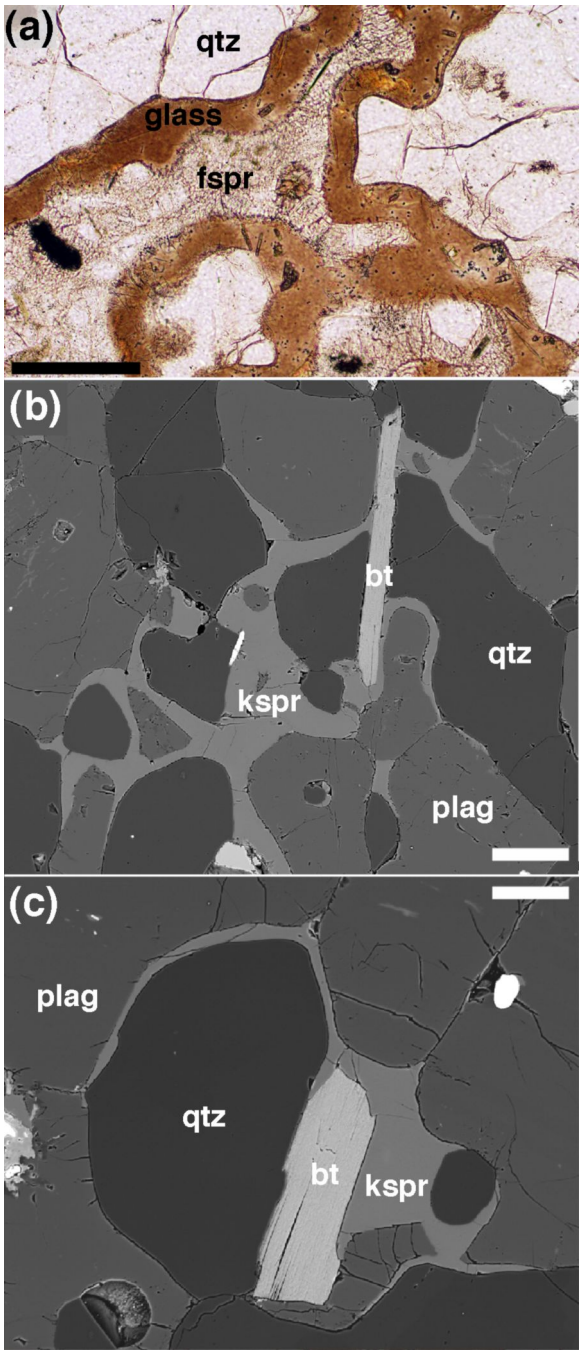

Melt rims from the aureole of the Glenmore plug, Ardnamurchan, separating polycrystalline quartz patches from partially melted (sieve-textured) feldspar (Holness *et al.*, 2005b). There are no indentations where any of the quartz-quartz grain boundaries meet the melt film; the effective dihedral angle is 180˚. Scale bar is 200 μm long. (b) and (c) Migmatite from the Ashuanipi Province, Quebec (sample number DL97-1006A), in which the melt (formed by the reaction biotite + plagioclase + quartz = orthopyroxene + melt; Sawyer, 2001) has been pseudomorphed by K-feldspar. Note how the melt films separate reacting phases, foming low dihedral angles where the propagating melt films pinch out. Scale bar 50 μm long in both images.

Solid-solid-solid dihedral angles

The variation of solid-state angles during prograde events is a relatively neglected topic, despite its potential for constraining thermal history (e.g. Harker and Parker, 1945) and its importance in interpreting the effects of recrystallisation and over-printing of microstructures formed in the presence of melt. During reaction in the solid state (i.e. metamorphic reactions forming new solid phases) one might expect the dihedral angles between grains of the product phases to be formed by the expediencies of crystal growth and replacement: angles will be determined more by the easiest crystal faces to grow, rather than by interfacial energies (Figure 5). This is borne out by variations in the population of true dihedral angles at three-grain junctions in quartzites. Voll (1969) measured quartz-quartz-quartz junctions in sedimentary rocks and found that they varied considerably (<60 – 180˚, as reported by Leibl *et al.*, 2007) about the median value of 120˚. The spread of angles decreases during metamorphism: triple junction angles in deformed quartz aggregates which have undergone dynamic recrystallisation and annealing have a narrower spread of 65 - 178˚ (Leibl *et al.*, 2007), and this is reduced to 97 – 144˚ in texturally equilibrated granulites (Vernon, 1968). This reduction of the spread is likely to reflect an approach to equilibrium of an initially non-equilibrated distribution and has potential for quantification of thermal histories.

The morphology of forsterite grains formed as a result of contact metamorphism of silicic dolomites by the Beinn an Dubhaich granite changes as a function of distance from the forsterite-in isograd. Grains at the isograd are commonly cuspate and irregular, while those closer to the granite are rounded. This change in morphology is accompanied by an increase in median (apparent) dihedral angle from 105˚ to 165˚ (Holness *et al.*, 1989). The low median values near the isograd have been interpreted as a consequence of the olivine pseudomorphing an original fluid-filled porosity (Holness *et al.*, 1989; Holness *et al.*, 1991) although it is possible that they preserve an early disequilibrium population formed during rapid reaction. The variation of angles towards the contact is

interpreted as progressive textural equilibration, and analysis of the variation suggests the data are consistent with equilibration via a diffusive process (Holness *et al.*, 1991).

Figure 5. Solid-solid-solid dihedral angles during metamorphic reaction

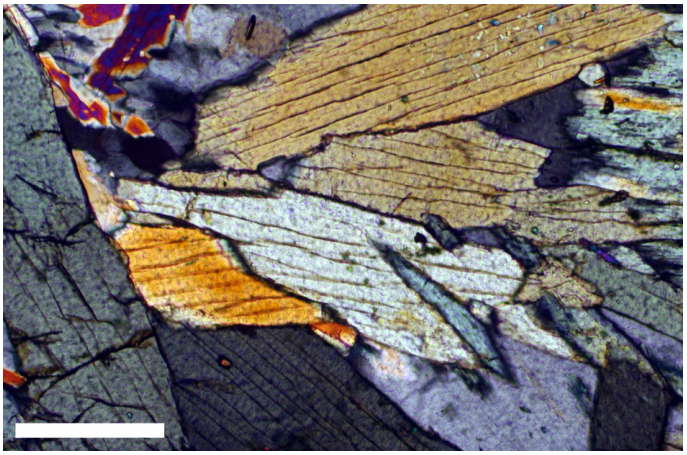

Glaucophane eclogite, Syros. The angles formed at three-grain junctions are created during reaction and have no bearing on the balancing of interfacial energies. Sample 97666 from the Harker collection, Cambridge University. Scale bar is 200 μm long.

Dihedral angles during retrograde events

We need to consider both the melt-solid-solid dihedral angle and the solid-solid-solid dihedral angles. Consideration of the latter is important because we are generally presented with a *fait accompli* in that all plutonic rocks, and many volcanic rocks are completely crystalline – we need to be able to interpret the record left in the dihedral angles. For this we need to understand how three-grain junctions are formed during solidification.

Melt-solid-solid dihedral angles

Melt-solid-solid angles in actively crystallizing systems generally vary between the two end-points of impingement (Elliott *et al.*, 1997; Holness *et al.*, 2005a) and equilibrium (Figure 6). During active crystallization, the random impingement of planar-sided grains results in a melt-solid-solid dihedral angle population with a high standard deviation (20-30˚) and a median of ~ 60˚ (since the internal angles of a triangle sum to 180˚). The angle distributions of samples K96-006 and Kameni (Figure 2, Table 2) are typical of impingement textures, and are distinct from those in equilibrated rocks (c.f. Figure 3). Holness *et al.* (2005a) demonstrate that the dihedral angle populations in a single suite of crystal-rich enclaves form a continuum between the two endpoints during textural equilibration of the sub-volcanic crystal mush. The population of dihedral angles varies smoothly from the original impingement texture to equilibrium (typically 20-30˚ with low standard deviation) in a continuous progression. The angle population therefore gets narrower as it approaches equilibrium. Exactly where an individual enclave sits on this spectrum depends on the relative rates of crystal growth and textural equilibration - this has not yet been quantified.

Figure 6. Impingement vs. equilibrium in glassy nodules

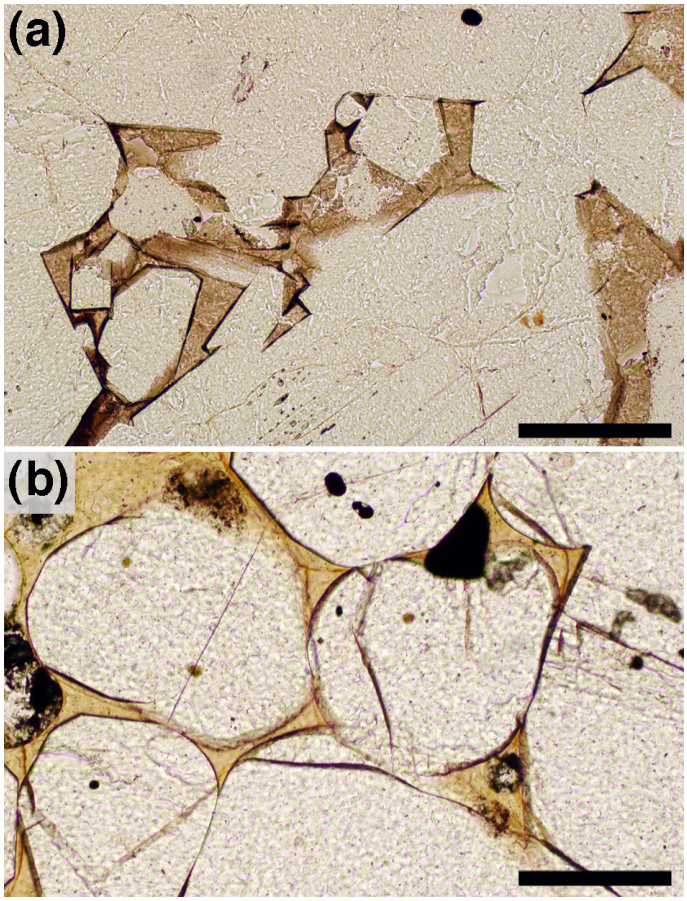

(a) glassy gabbroic nodule entrained in a basaltic lava flow, Iceland. The plagioclase crystals (clear) are randomly juxtaposed, with their planar growth faces making widely varying angles at the corners of the melt-filled pores (brown glass). Scale bar is 200 μm long. (b) Glassy nodule entrained in basaltic flow, Hawaii. The olivine grains (clear) are rounded, with smoothly curved interfaces against the melt (brown glass). The equilibrium melt-olivine-olivine dihedral angle is developed at pore corners. Scale bar is 200 μm long.

Consideration of melt-solid-solid dihedral angles must take into account the possibility that diffusion-limited growth may significantly modify the geometry of pore corners. During active growth within a crystal framework the rate of growth of the solid phase near pore junctions decreases as the nearby melt becomes depleted in the necessary chemical components. This limitation is less marked for those parts of the grain further from the junction – these can therefore continue to grow. The effect of this localized diffusion-limited growth is to create curved solid-melt interfaces and a lower dihedral angle (Figure 7). The angle distribution is indistinguishable from those formed by progressive textural equilibration in melt-bearing enclaves (Holness *et al.*, 2005c). The two processes of textural equilibration and diffusion-limited growth can be distinguished if the pore walls display evidence of growth instabilities and protuberances characteristic of diffusion-limited growth.

Figure 7. The effects of diffusion-limited growth at pore corners

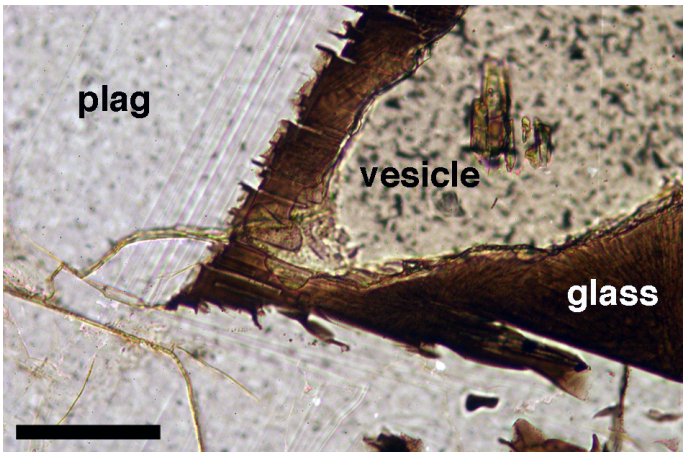

Detail of the junction between two plagioclase grains in a glassy nodule from the Kameni Islands, Santorini. Note the progression of the growth faces, marked by faint lines in the margins of the plagioclase grains. Progressive starvation of the plagioclase grains in the immediate vicinity of the two-grain junction, due to the limitations imposed on growth by diffusion in the melt, have resulted in curvature of the plagioclase-melt interface. A distinction can be made between this and true textural equilibration because here diffusion-limited growth has also resulted in destabilization of the plagioclase-melt interface, leading to growth of protuberances. The scale bar is 200 μm long.

Solid-solid-solid dihedral angles

Solid-solid-solid dihedral angles formed during cooling of melt-bearing rocks are formed during solidification. Microstructures in solidified igneous rocks have been the subject of considerable attention and depend on cooling rate and the order in which the liquid becomes saturated in the various solid phases (e.g. Wager *et al.*, 1960; Hunter, 1987; 1996; Vernon, 2004). The simplest system (although not widely applicable) is that in which only a single phase nucleates and grows – here solidification involves growth and impingement of individual crystals. Elliott *et al.* (1997) investigated the angle distribution formed by the growth and impingement of isotropic single-phase aggregates using computer simulations. They demonstrated that the population of apparent angles measured in a 2-D section through an artificially grown aggregate has a median of 120˚ and a spread very similar to that of a normal distribution of true angles with a standard deviation of 20˚. They did not present the populations of true angles so their results cannot be compared directly with those of Voll (1960).

In systems in which more than one phase crystallizes, the phase arriving first on the liquidus generally forms grains with a shape controlled variably by kinetic constraints (leading to growth facets) or minimization of interfacial area (leading to shapes with variable proportions of curved and planar surfaces, depending on the degree of anisotropy of interfacial energy). The balance between these two end-members depends on the relative rates of crystal growth and textural equilibration – this has not yet been quantified but has potential to constrain cooling rates of phenocryst-bearing magmas. If sufficient grains accumulate they may aggregate to form a framework before the next phase arrives on the liquidus. In such a case the second phase nucleates and grow in the pore spaces. Clearly, as more phases are added to the liquidus assemblage solidification progressively involves simultaneous growth of an increasing number of phases. Elimination of the remaining melt between grains, and therefore the establishment of the initial solid-solid-solid dihedral angle, is a complex interaction between the competing phases at the junction and involving transfer of unwanted chemical species to other growth sites (Figure 8). The details of this process are currently poorly understood.

To date all attention has been focused on slowly cooled melt-bearing rocks, primarily perhaps because the grain size is sufficiently large that meaningful observations can be easily made. It is clear that in many rocks formed by solidification over long time scales (i.e. plutonic igneous rocks and regional migmatite terrains)

microstructures are typified by low solid-solid-solid dihedral angles.

Much of the published work on dihedral angles in igneous rocks has been concentrated on augite-plagioclase-plagioclase junctions in gabbros (e.g. Holness *et al.*, 2007a; Holness and Winpenny, 2009). The angle populations in shallow crustal mafic intrusions are generally far from equilibrium, with medians as low as 65-70˚ and standard deviations of the order 25˚. These low angles are explained as a consequence of the augite infilling and pseudomorphing the original melt-filled porosity, inheriting the impingement texture (Figures 9a, b, c; Holness *et al.*, 2005a). Gabbros containing angles with a higher median and lower standard deviation (Figures 9d, e, f) are thought to have undergone significant sub-solidus textural re-equilibration of the augite-plagioclase-plagioclase junctions (Holness *et al.*, 2005a). An alternative possibility is that slower cooling resulted in simultaneous growth of plagioclase and augite at the junction (e.g. Figure 8a) and hence a higher angle.

The other type of slowly cooled rock that has been studied extensively is migmatite. Solidified melt pools in migmatites are typified by cuspate grains with low dihedral angles (Figure 10) thought to have formed by pseudomorphing of an original melt-filled pore by phases crystallizing from the melt (e.g. Platten, 1981; Harte *et al.*, 1993; Sawyer, 1999; Clemens and Holness, 2000; Holness and Sawyer, 2008). The current explanation for this phenomenon is based on the effect of pore size on crystal nucleation and growth.

Figure 8. The infilling of melt-filled pores during solidification

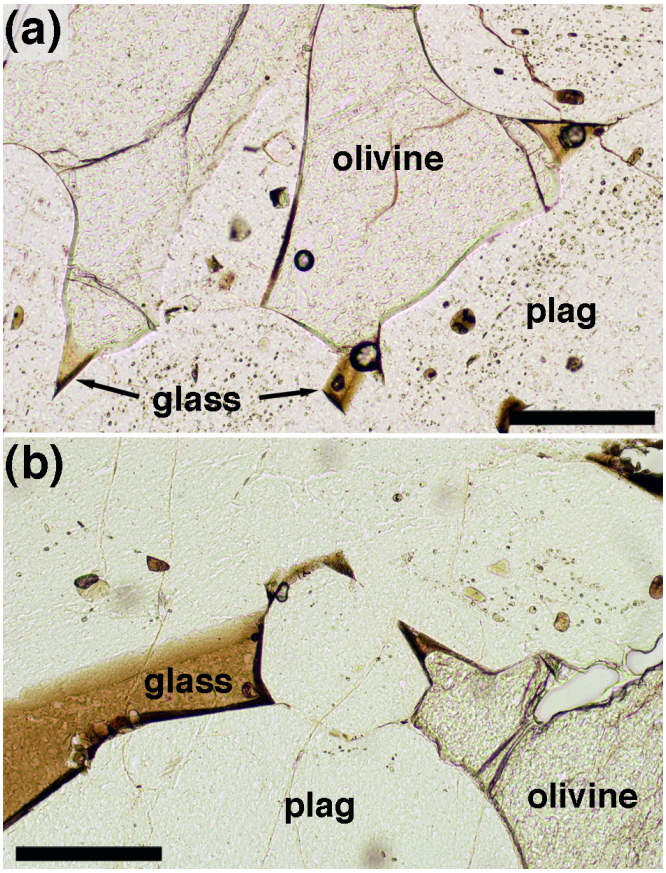

Glassy olivine gabbro nodules entrained in a lava flow, Iceland, illustrating the details of melt pockets partially infilled by olivine. Scale bars in both images are 200 μm long. (a) Note how the olivine-plagioclase grain boundaries curve towards the planar-sided pockets of melt (now glass), indicating simultaneous growth of both phases. (b) The olivine grain appears to be growing towards the plagioclase-plagioclase junction with little or no associated growth of the plagioclase. If this were to continue to completion, the olivine would inherit the impingement angle.

Figure 9. Textural progression in gabbros

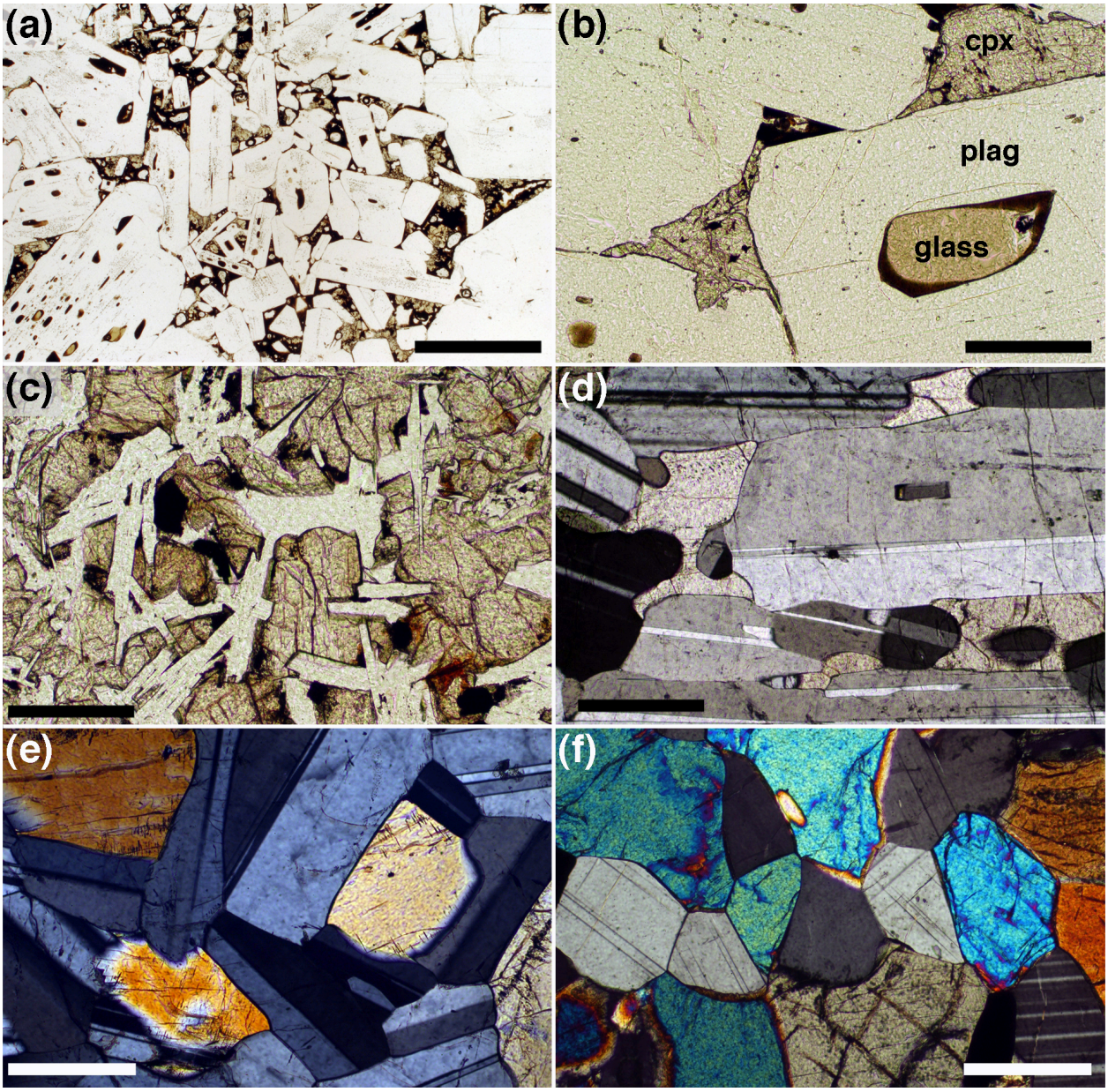

Images of gabbros showing the progression from the melt-bearing stage with active solidification and crystal growth to solid-solid-solid textural equilibrium. (a), (b) and (c) Glassy gabbro nodules entrained in basaltic lava flow, Iceland. (a) Impingement texture formed by random juxtaposition of plagioclase primocrysts. The spaces between are filled variously with glass, vesicles and augite. Scale bar is 1 mm long. (b) Detail of gabbro nodule showing augite partially infilling the space between the plagioclase grains, inheriting the impingement angle in three places, while melt remains at the fourth. Scale bar is 200 μm long. (c) Almost fully solidified gabbroic clot in basaltic lava. Note the randomly oriented plagioclase grains and the impingement angles inherited by the augite. Scale bar is 200 μm long. (d) Troctolitic gabbro from the Eastern Layered Series, Isle of Rum, with interstitial augite. This is sample A041 from the Unit 9 allivalite, subjected to metasomatic infiltration of primitive melt (Holness, 2005; Holness *et al.*, 2007b). The median augite-plagioclase-plagioclase dihedral angle in this sample is 84˚. Scale bar is 200 μm long. (e) Gabbroic cumulate, Rum, in which the augite-plagioclase-plagioclase dihedral angle is intermediate between that of impingement and solid-solid textural equilibrium. Scale bar is 200 μm long. (f) Granulite, sample 11787 from the Harker Collection of Cambridge University. The augite-plagioclase-plagioclase dihedral angle population in this sample is in textural equilibrium (see Table 2 for details). Scale bar is 200 μm long.

Figure 10. Cuspate grains in migmatite

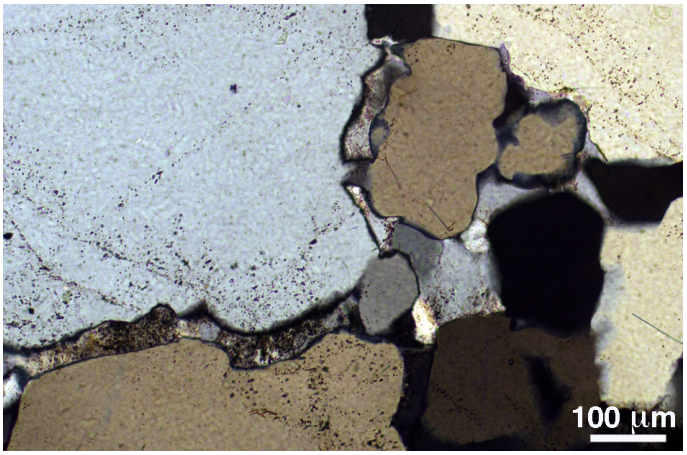

Quartz-feldspathic migmatite from the aureole of the Ballachulish Complex, Scotland. The (dusty) feldspar forms cuspate grains on quartz-quartz grain boundaries and at quartz three-grain junctions, indicative of crystallization from a melt phase.

Because the free energy of an interface is a function of its curvature, the supersaturation required to stabilize a small grain growing from a liquid is greater than that required for a larger grain (Cahn, 1980; Adamson, 1990). This effect is what drives Ostwald ripening during initial growth of crystals in a liquid, and means that solidification of a melt phase in a small pore occurs at a lower temperature (i.e. a greater undercooling) than that in a large pore (e.g. Bigg, 1953; Melia & Moffitt, 1964; Cahn, 1980; Scherer, 1999; Putnis and Mauthe, 2001; Cesare *et al.*, 2009). It means that the continued growth of the olivine grains into the melt-filled pockets shown in Figure 8 requires greater and greater departures from equilibrium (i.e. undercooling) since this growth requires the reduction of the radius of curvature of the olivine-melt interface. The consequence of this delay in crystal growth in the smallest pores means that instead of the simultaneous growth of several phases seen in the larger pores (and as described by the equilibrium phase diagram), small pores tend to crystallise by initial overgrowth of the pore walls followed by nucleation and growth of another phase in the remaining pore space (Holness and Sawyer, 2008). If there is sufficient delay before the pore is pseudomorphed, textural equilibration may occur, leading to the pseudomorph inheriting a low dihedral angle and thus the cuspate grain shape so typical of migmatites (Figure 11).

Figure 11. Sequential crystallization in poly-saturated melts

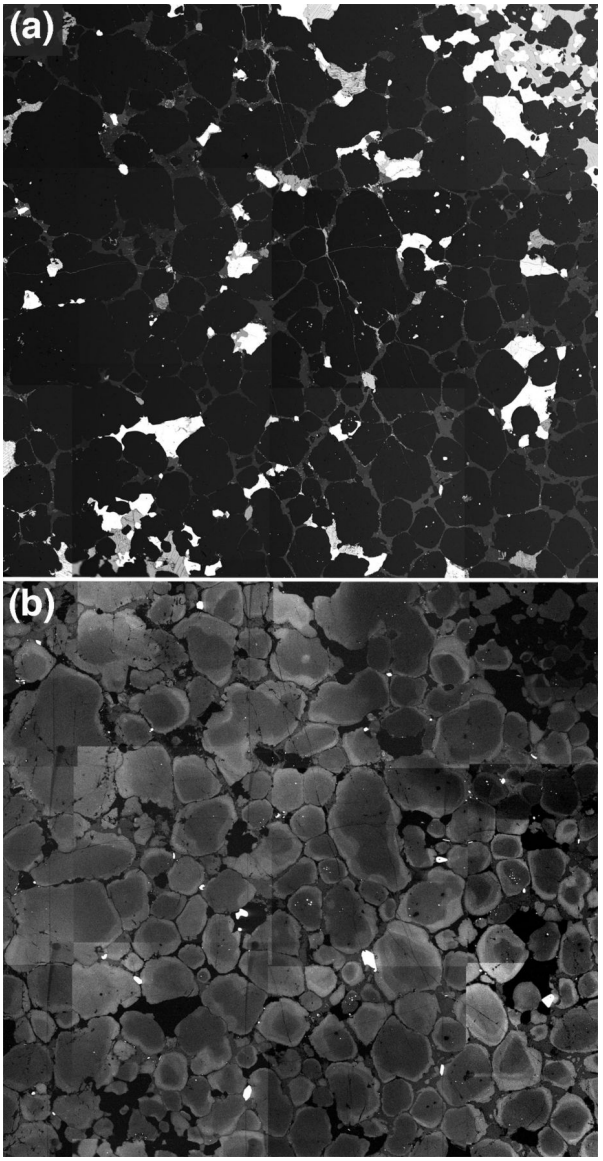

(a) BSE image and (b) CL image of a sample of Fe-oxide, plagioclase and amphibole bearing quartzite from the Biwabik Formation, metamorphosed at 2kbar in the western part of the aureole of the Duluth Igneous complex, Minnesota. The BSE image shows the distribution of the plagioclase (pale grey) and the rounded quartz grains (dark grey), with oxide and amphibole grains (white). Note how the morphology of the plagioclase mimics that expected for a texturally equilibrated melt phase. (b) The same area imaged in CL. As an approximate guide, the brightness of the quartz in CL correlates with the temperature at which it crystallized. Thus the dark cores are restitic while the bright rims crystallized at high temperatures. From this it becomes clear that the quartz component of the melt phase has overgrown the restitic quartz grains, leaving the plagioclase to crystallise and pseudomorph the remaining porosity. Both images are 1cm across.

Does rock fabric have an effect on disequilibrium dihedral angle populations?

Figure 12. The effects of fabric on dihedral angles

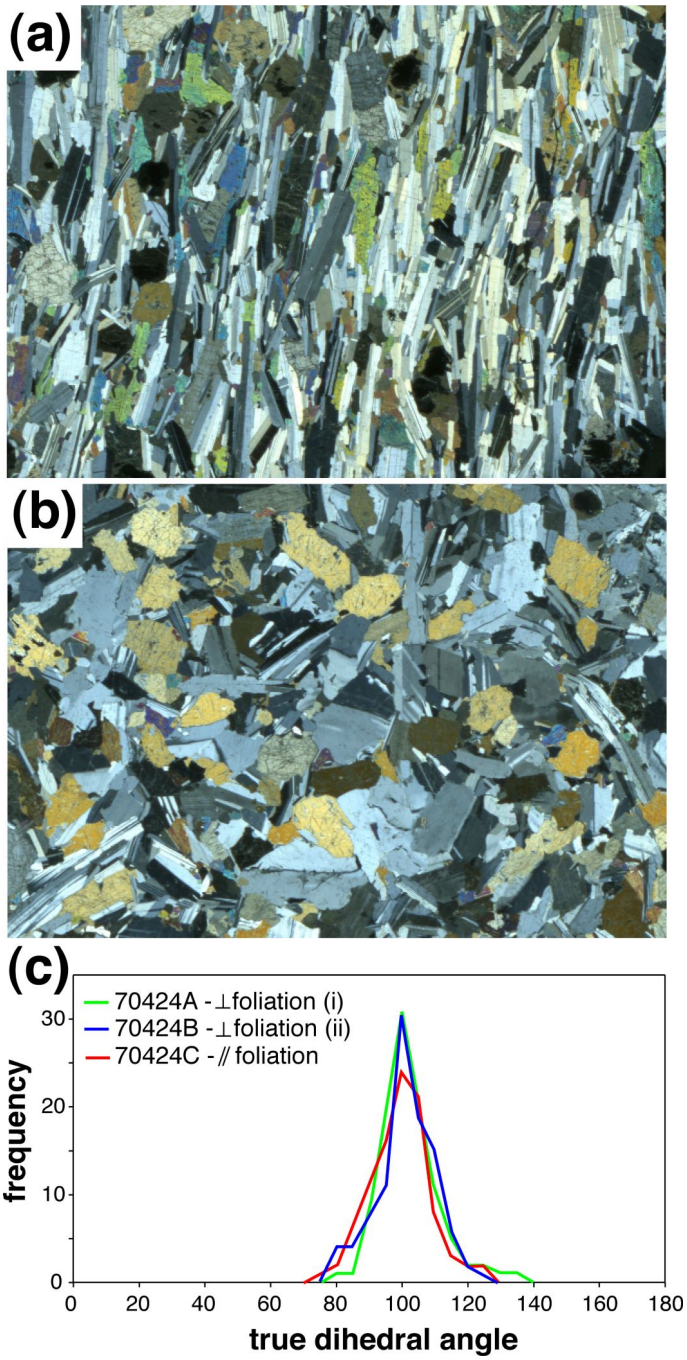

(a) Foliated gabbro from the Stillwater Intrusion, Montana, cut perpendicular to foliation (sample 70424A). (b) The same sample, cut parallel to the foliation (sample 70424C). Both images are 24mm across. (c) Frequency of true augite-plagioclase-plagioclase dihedral angles in three mutually orthogonal thin sections of sample 70424. See Table 6 for statistical analysis of the results.

It is well understood that the melt topology and permeability of melt-bearing texturally equilibrated rocks with a strong fabric (a preferred mineral orientation) can be strongly anisotropic if one or more of the minerals in the rock is anisotropic with respect to interfacial energies (Waff and Faul, 1992; Laporte and Watson, 1995). However, the question of whether such an effect also exists in a non-equilibrated rock with a strong fabric has not yet been properly addressed. A preliminary attempt was made to investigate this, using a strongly foliated two-pyroxene gabbro from the Stillwater Intrusion Montana (sample 70424 from the Cambridge Harker Collection). Three mutually orthogonal sections were cut from this rock, two perpendicular to the foliation and one in the plane of the foliation. Up to 100 measurements were made of augite-plagioclase-plagioclase dihedral angles in each section (Figure 12). The median and standard deviations for these three populations are shown in Table 2, with errors on the median determined according to the method of Stickels and Hücke (1964). The median is the same within error for the three samples, and the standard deviation is also very similar.

Determination of whether two populations taken from different specimens differ significantly requires a non-parametric method if we don't know the distribution functions of the angles in the two samples. Several of these exist, including Mood's median test (now commonly regarded as obsolete), the Kolmogorov-Smirnov test and the Mann-Whitney U test.

The Kolmogorov-Smirnov test examines the maximum difference, *D*, between two data sets on a cumulative frequency plot and calculates the probability, *P*, that they come from the same underlying population. According to this test, the two datasets from the sections perpendicular to the foliation are more similar to each other than they are to the population of angles measured parallel to the foliation (Table 6). This result is backed up by the Mann-Whitney U test. The values of *U* for the pair of samples oriented perpendicular to the foliation are close to that expected for the null hypothesis (i.e. the hypothesis that the two populations are the same), while that for the pairs of samples each containing one perpendicular and one parallel to the foliation are further from that expected for the null hypothesis (Table 6). The (two-tailed) probability that the two samples perpendicular to the foliation are the same is higher than that for the other two pairings. However, the probabilities are all sufficiently

high that the null hypothesis is still likely to be true (i.e. $P >> 0.05$).

These two statistical tests demonstrate measurable differences between the dihedral angle populations measured perpendicular and parallel to the foliation in this Stillwater gabbro, even though the median and standard deviations are indistinguishable. Although the observed effect is not important enough to affect studies based on comparisons of the median values (e.g. Holness *et al.*, 2007a), the differences warrant further work to obtain a full understanding of the effects of crystalline anisotropy on disequilibrium dihedral angle populations.

Table 6. Comparison of augite-plagioclase-plagioclase dihedral angle populations

Kolmogorov-Smirnov test			**Mann-Whitney U test**			
	D	*P*			U for null hypothesis	Two-tailed probability *P*
A : B	0.1	0.677	$U_A = 5069$	$U_B = 4931$	5000	0.865
A : C	0.149	0.208	$U_A = 4268$	$U_C = 5432$	4850	0.1471
B : C	0.127	0.384	$U_B = 4269$	$U_C = 5431$	4850	0.1471

Statistical data for the comparison of augite-plagioclase-plagioclase dihedral angle populations measured in three mutually orthogonal thin-sections of a foliated gabbro from the Stillwater Intrusion, Montana. Sections A and B were cut perpendicular to the plane of the foliation while C was cut parallel to the plane of the foliation.

Textural Equilibration

Textural equilibration generally starts at grain boundaries, and in particular at three-grain junctions where the dihedral angle adjusts to the equilibrium value. This sets up a change in curvature near the junction that propagates outwards (Figure 13), creating a surface of constant mean curvature along the entire interface (Voll, 1960). Once the grains have attained their minimum energy shape (which includes a certain area of planar faces due to the inherent anisotropy of most rock-forming minerals, e.g. Figure 1b), the microstructure will then evolve towards a unimodal grain size by coarsening (Higgins, 2010). The mechanisms by which this equilibration process occurs are diffusive, and therefore occur more rapidly at higher temperatures (Holness *et al.*, 1991) and in finer-grained rocks. Equilibration is also faster in the presence of fluid phase, either H_2O (Holness *et al.*, 1991) or a silicate melt. The effect of H_2O in enhancing diffusion, even in vanishingly small concentrations (<<0.1 wt. %) at which the H_2O molecules are likely to be adsorbed on grain boundaries rather than forming a free phase, is well known, with major effects on metamorphic reaction textures. The presence of H_2O may also enhance rates of grain boundary migration (Schenk and Urai, 2004). Mass transport in melt-filled pockets is higher than on dry grain boundaries, so melt-filled pores reach equilibrium relatively rapidly.

Most rocks with well-equilibrated microstructures are granulites (Figure 9f) and hornfelses. Textural equilibrium is also commonly seen in mono-mineralic rocks at lower grades such as carbonates and quartzites (e.g. Figure 1a). This is because it is much easier to re-organise grain boundaries by movement of material across them (only possible if the two grains on either side are of the same phase) compared to moving material along them (necessary for inter-phase boundaries). The requirement for grain boundary diffusion is also the reason why fine-grained poly-phase aggregates equilibrate faster than their coarse-grained equivalents .

Because the process of equilibration is diffusive, the critical parameter for equilibration is the time-integrated thermal history. Thus rocks need to be held at sufficiently high temperatures (in the absence of reaction or deformation) for a long time. This means that while a gabbroic cumulate may solidify at temperatures well above 1100˚C it is possible that the augite-plagioclase-plagioclase dihedral angles change little from those originally inherited from the original solidification, whereas a granulite may be completely texturally equilibrated despite

not having been heated above 900˚C. The critical difference between the two is the period over which they remained hot. The granulite may have been at high temperatures for 10^6 years, while typical km-scale crustal gabbroic intrusions cool to ambient temperatures over 10^5 years.

Figure 13. Dihedral angles are the first sign of textural modification

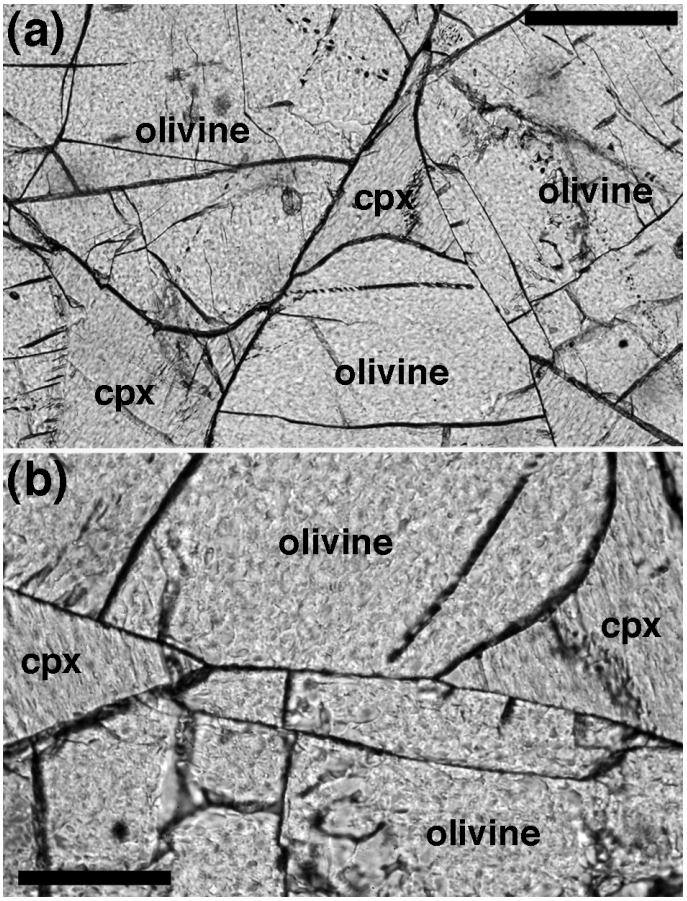

Cumulus olivine grains enclosed by an augite oikocryst. Eastern Layered Intrusion, Rum. (a) Note how the dihedral angle is larger than expected from extrapolation of the curved interfaces far from the junction itself. Scale bar is 200 μm long. A pair of augite-olivine-olivine junctions from (a) is enlarged in (b). Scale bar is 100 μm long. The dihedral angles in this oikocryst were analysed by Holness *et al.* (2005a) and this photomicrograph shows a central part of the oikocryst.

A useful concept, used extensively for diffusive processes (e.g. re-setting of isotopic ratios), is the closure temperature – that temperature at which mass transfer by diffusion becomes so slow that it effectively ceases to make significant differences to the microstructure. In a similar way to that for isotope ratios, the closure temperature is sensitive to the cooling rate. Rocks that are rapidly cooled have a higher closure temperature for microstructural change than rocks that were more slowly cooled. This means that it is possible to quench relatively unmodified microstructures in a km-scale gabbro body intruded into the shallow crust, while a rock that reached a lower maximum temperature may approach textural equilibrium more closely.

A measure of the closure temperature, and an indication of the timescales for dihedral angle modification, is provided by Holness *et al.* (2005a). The augite-olivine-olivine- dihedral angles in a cluster of three contiguous augite oikocrysts in a peridotite from the Rum Eastern Layered Intrusion decrease from the centres to the edges of the oikocryst. The population of angles around the edges of the oikocryst is similar to that observed in texturally equilibrated melt-bearing olivine aggregates, while that in the centre is closer to that expected for equilibrated augite-olivine-olivine junctions. Holness *et al.* (2005a) interpret the data as an indication that the augite-olivine-olivine angle inherited an equilibrated melt-olivine-olivine angle that then was modified towards the higher angles expected for augite-olivine-olivine equilibrium. That the angle changes from the centres to the edges demonstrates not only that this process was occurring during the growth of the oikocryst itself, but that it effectively stopped during the last stages of oikocryst growth: the closure temperature for dihedral angle change was therefore close to that at which the oikocryst stopped growing, and may have been of the order 1000˚C.

A similarly high closure temperature is indicated by Harte *et al.* (1993) who report bimodal populations of ilmenite-olivine-olivine angles in the Matsuko peridotites (a suite of xenoliths entrained by a kimberlite). The low angles are interpreted as an inheritance from a melt-bearing precursor. Although we don't know the precise history of these xenoliths their mantle source is indicative of high temperatures and thus a high closure temperature for dihedral angle modification.

Case study: The variation of dihedral angles in layered intrusions

An example of information which can be obtained from a detailed examination of dihedral angles in non-equilibrated rocks is provided by the body of work done

on layered gabbroic intrusions by M.B. Holness and co-workers. This work concentrates on the augite-plagioclase-plagioclase angle because three-grain junctions between these two phases tend to be fresh and unaltered (in contrast to those involving olivine) and because these two phases occur throughout many layered mafic intrusions, even those in which fractionation has reached the extreme endpoint (e.g. Skaergaard). Most of the published work is based on comparisons of the median value of the population of augite-plagioclase-plagioclase dihedral angles, Θ_{cpp}. The value of Θ_{cpp} lies between the original value inherited during solidification from an impingement texture (60 – 70˚) and that pertaining to a texturally equilibrated solid (114˚).

Within a single intrusion, Θ_{cpp} correlates with the liquidus assemblage of the cumulate (Holness *et al.*, 2007a, 2007c). In the Skaergaard intrusion, comprising a continuous succession of increasingly fractionated floor cumulates, Θ_{cpp} increases in a step-wise fashion at the arrival of each of the cumulus phases augite, Fe-Ti oxides and apatite (Holness *et al.*, 2007a; 2007c). The Rum Eastern Layered Series comprises an alternating series of olivine cumulates and plagioclase-bearing cumulates on a 1-50m scale (Emeleus *et al.*, 1996). The latter form layers up to 40m thick of either gabbros (with cumulus plagioclase, olivine and augite) or troctolites (with only plagioclase and olivine as cumulus phases). The value of Θ_{cpp} in the troctolites is ~ 80˚, while that in the gabbros is ~90˚ (Holness, 2005; Holness *et al.*, 2007c).

At first sight one might suspect that the dihedral angles at augite-plagioclase junctions in mafic cumulates have a compositional control. However, that the control is primarily thermal is illustrated by the troctolitic cumulates underlying an intrusive peridotite sill in the Eastern Layered Intrusion of Rum (Holness, 2005). The Θ_{cpp} values in the troctolite increase over a few metres towards the peridotite body, from ~ 80˚ to ~100˚. The mineral assemblage in the troctolite remains the same, so the increase in angle must be a consequence of the greater opportunity for textural equilibration in the aureole of the peridotite sill, in a similar fashion to the varying angle population through a single oikocryst.

The step-wise changes in Θ_{cpp} at the arrival of a new liquidus phase in Skaergaard, and the bimodal Θ_{cpp} in the alternating Rum cumulates have been explained using the concept of fractional latent heat (Holness *et al.*, 2007a). The loss of heat from a body of magma is controlled by conduction through the walls, roof and floor. However, in the temperature interval over which crystallisation occurs, there are two sources of heat contributing to the enthalpy budget: the sensible heat (the actual temperature of the body) and the latent heat of crystallisation. The fraction of the enthalpy budget that is provided by latent heat is known as the fractional latent heat, and this increases through the crystallization interval, reaching unity at the terminal eutectic point (Holness *et al.*, 2009). The increase in fractional latent heat is step-wise at the arrival of each new phase on the liquidus. Holness *et al.* (2007a) suggest that the step-wise increases in Θ_{cpp} reflect this change in fractional latent heat, due to a corresponding decrease in the rate at which the sensible heat falls during crystallization. The cumulates keep hotter for longer, thus permitting an increase in the dihedral angle.

Conclusions

The impetus for studies of dihedral angles came from metallurgists interested in predicting the behaviour of composite materials and alloys. Their work was noticed by Earth scientists who realized that textural equilibrium might control melt migration in the mantle. Much of the early petrographic work was therefore aimed at understanding textural equilibrium, and determining equilibrium values of the dihedral angle. However, a cursory look at most crustal igneous and metamorphic rocks demonstrates that textural equilibrium is actually rather rare; dihedral angles are generally out of equilibrium. The potential for this disequilibrium can only be realized by studies determining the true distribution of these angles, and in practical terms this means using a universal stage. At present we are in the earliest stages of putting disequilibrium dihedral angles to good use, and almost all published work is purely qualitative, based on comparison of dihedral angle populations from a large number of well-located samples. Full exploitation of the observations can only be achieved if we make the next step forward into quantitative studies. We need to develop not only an understanding of the processes leading to the initial dihedral angle distribution but also an understanding of the processes and rates of its subsequent modification in either the super- or the sub-solidus. Future work should be aimed at solving these problems.

Acknowledgements

I am indebted to many people who have drawn my attention to important questions relating to dihedral angles, including Troels Nielsen, Madeleine Humphreys, Dan McKenzie, Mike, Bickle, Michael Higgins, Mike Cheadle and numerous anonymous reviewers of my previous papers. Helpful comments from Ron Vernon helped clarify an earler version of the manuscript.

References

Adamson, A.W. (1990) Physical chemistry of surfaces, 5th edition. Wiley, New York.

Bagdassarov, N., Golabek, G.J., Soferine, G. & Schmidt, M.W. (2009) Constraints on the Fe-S melt connectivity in mantle silicates from electrical impedance measurements. Physics of the Earth and Planetary Interiors 177: 139-146, 10.1016/j.pepi.2009.08.003

Bai, Q., Jin, Z.-M., & Green, H.W. (1997) Experimental investigation of the rheology of partially molten peridotite at upper mantle pressures and temperatures. In: Deformation-enhanced fluid transport in the Earth's Crust and Mantle (ed: Holness MB) pp. 40-61. Chapman & Hall, London.

Ballhaus, C.H., & Ellis, D.J. (1006) Mobility of core melts during Earth's accretion. Earth and Planetary Science Letters 143: 137-145 10.1016/0012-821X(96)00135-5

Beere, W. (1975) A unifying theory of the stability of penetrating liquid phases and sintering pores. Acta Metallurgica 23: 131-145, 10.1016/0001-6160(75)90078-4

Bigg, E.K. (1953) The supercooling of water. Proceedings of the Physical Society (London) 66B: 688-694.

Borsch, R.S. & Green, H.W. (1990) Experimental investigation of the rheology and structure of partially molten lherzolite deformed under upper mantle pressures and temperatures. EOS (American Geophysical Union) Transcations 71: 629.

Brenan, J.M. & Rose, L.A. (2002) Experimental constraints on the wetting of chromite by sulfide liquid. The Canadian Mineralogist 40: 1113-1126, 10.2113/gscanmin.40.4.1113

Bulau, J.R., Waff, H.S. &, Tyburczy, J.A. (1979) Mechanical and thermodynamic constraints on fluid distribution in partial melts. Journal of Geophysical Research 84: 6102-6107, 10.1029/JB084iB11p06102

Cahn, J.W. (1980) Surface stress and the chemical equilibrium of small crystals: I. The case of the isotropic surface. Acta Metallurgica 28: 1333-1338, 10.1016/0001-6160(80)90002-4

Cesare, B., Ferrero, S., Salvioli-Mariani, E., Pedron, D. & Cavallo, A. (2009) "Nanogranite" and glassy inclusions: the anatectic melt in migmatites and granulites. Geology 37: 627-630, 10.1130/G25759A.1

Cesare, B., Mariani, E.S., & Venturelli, G. (1997) Crustal anatexis and melt extraction during deformation in the restitic xenoliths of El Johazo (SE Spain). Mineralogical Magazine 61: 15-27, 10.1180/minmag.1997.061.404.03

Cheadle, M.J., Elliott, M.T., & McKenzie, D. (2004) Percolation threshold and permeability of crystalising igneous rocks: the importance of textural equilibrium. Geology 32: 757-760, 10.1130/G20495.1

Clemens, J.D & Holness, M.B. (2000) Textural evolution and partial melting of arkose in a contact aureole: a case study and implications. Electronic Geosciences 5: 4.

Cmíral, M., Fitz Gerald, J.D., Faul, U.H. & Green, D.H. (1998) A close look at dihedral angles and melt geometry in olivine-basalt aggregates: a TEM study. Contributions to Mineralogy and Petrology 130: 336-345.

Dimanov, A., Dresen, G. & Wirth, R. (1998) High-temperature creep of partially molten plagioclase aggregates. Journal of Geophysical Research 103: 9651-9664, 10.1029/97JB03742

Elliott, M.T., Cheadle, M.J. & Jerram, D.A. (1997) On the identification of textural equilibrium in rocks using dihedral angle measurements. Geology 25; 355-358, 10.1130/0091-7613(1997)025<0355:OTIOTE>2.3.CO;2

Emeleus, C. H., Cheadle, M. J., Hunter, R. H., Upton, B. G. J., & Wadsworth, W. J. (1996) The Rum Layered Suite. In Layered Intrusions (ed. R.G. Cawthorn), Developments in Petrology 15.: 403-439. The Netherlands: Elsevier.

Fujii, N., Osamura, K., & Takahaski, E. (1986) Effect of water saturation on the distribution of partial melt in the olivine-pyroxene-plagioclase system. Journal of Geophysical Research 91: 9253-9259, 10.1029/JB091iB09p09253

Gaetani, G.A. & Grove, T.L. (1999) Wetting of mantle olivine by sulphide melt: implication for Re/Os ratios in mantle peridotite and late-stage core formation. Earth and Planetary Science Letters 169: 147-163.

Gleason, G.C., Bruce, V. & Green, H.W. (1999) Experimental investigation of melt topology in partially molten quartzo-feldspathic aggregates under hydrostatic and non-hydrostatic stress. Journal of Metamorphic Geology 17: 705-722, 10.1046/j.1525-1314.1999.00228.x

Harker, D. & Parker, E.R. (1945) Grain shape and grain growth. Transactions of the American Society of Metals 34: 156-195.

Harte, B., Hunter, R.H. & Kinny, P.D. (1993) Melt geometry, movement and crystallization, in relation to mantle dykes, veins and metasomatism. Philosophical Transactions of the Royal Society of London A342: 1-21, 10.1098/rsta.1993.0001

Herring, C. (1951a) Some theorems on the free energies of crystal surfaces. Physical Review 82: 87-93, 10.1103/PhysRev.82.87

Herring, C. (1951b) Surface tension as a motivation for sintering. In: (Kingston, W.E., ed.) Physics of Powder Metallurgy, pp. 143-179. McGraw-Hill, New York.

Hier-Majumda, S. & Kohlstedt, D.L. (2006) Roel of dynamic grain boundary wetting in fluid circulation beneath volcanic arcs. Geophysical Research Letters 33: 10.1029/2006GL025716

Hier-Majumda, S., Richard, Y. & Bercovici, D. (2006) Role of grain boundaries in magma migration and storage. Earth and Planetary Science Letters 248: 735-749, 10.1016/j.epsl.2006.06.015

Higgins, M.D. (2006) Quantitative textural measurements in igneous and metamorphic petrology. Cambridge, UK, Cambridge University Press, 10.1017/CBO9780511535574

Higgins, M.D. (2010) Textural coarsening in igneous rocks. International Geology Review, in press.

Hiraga, T., Nishikawa, O., Nagase, T., Akizuki, M. & Kohlstedt, D.L. (2002) Interfacial energies for quartz and albite in pelitic schist. Contributions to Mineralogy and Petrology 143: 664-672, 10.1007/s00410-002-0375-4

Hirth, G. & Kohlstedt, D.L. (1995a) Experimental constraints on the dyniamics of the partially molten upper mantle: deformation in the diffusion creep regime. Journal of Geophysical Research 100: 1981-2001, 10.1029/94JB02128

Hirth, G. & Kohlstedt, D.L. (1995b) Experiemtnal constraints on the dynamics of the partially molten upper mantle 2: deformation in the dislocation creep regime. Journal of Geophysical Research 100: 15441-15449, 10.1029/95JB01292

Holness, M.B. (1993) Temperature and pressure dependence of quartz-aqueous fluid dihedral angles: the control of adsorbed H_2O on the permeability of quartzites. Earth and Planetary Science Letters 117: 363-377, 10.1016/0012-821X(93)90090-V

Holness, M.B. (1995) The effect of feldspar on quartz-H_2O-CO_2 dihedral angles at 4 kbar, with consequences for the behaviour of aqueous fluids in migmatites. Contributions to Mineralogy and Petrology 118: 356-364, 10.1007/s004100050020

Holness, M.B. (2005) Spatial constraints on magma chamber replenishment events from textural observations of cumulates: the Rum Layered Intrusion, Scotland. Journal of Petrology 46: 1585-1601, 10.1093/petrology/egi027

Holness, M.B. (2006) Melt-solid dihedral angles of common minerals in natural rocks. Journal of Petrology 47: 791-800, 10.1093/petrology/egi094

Holness, M.B., Anderson, A.T., Martin, V.M., Maclennan, J., Passmore, E. & Schwindinger, K., (2007c). Textures in partially solidified crystalline nodules: a window into the pore structure of slowly cooled mafic intrusions. Journal of Petrology 48: 1243-1264, 10.1093/petrology/egm016

Holness, M.B., Bickle, M.J. & Graham, C.M. (1991) On the kinetics of textural equilibration in forsterite marbles. Contributions to Mineralogy and Petrology 108: 356-367 10.1007/BF00285943

Holness, M.B., Bickle, M.J. & Harte, B. (1989) Textures of forsterite-calcite marbles from the Beinn an Dubhaich aureole, Skye, and implications for the structure of metamorphic porosity. Journal of the Geological Society of London 146: 917-920, 10.1144/gsjgs.146.6.0917

Holness, M.B. & Bunbury, J.M. (2006) Insights into continental rift-related magma chambers: igneous nodules from the Kula Volcanic Province, Western Turkey. Journal of Volcanology and Geothermal Research 153: 241-261, 10.1016/j.jvolgeores.2005.12.004

Holness, M.B., Cheadle, M.J. & McKenzie, D. (2005a) On the uses of changes in dihedral angle to decode late-stage textural evolution in cumulates. Journal of Petrology 46: 1565-1583, 10.1093/petrology/egi026

Holness, M.B., Dane, K., Sides, R., Richardson, C. & Caddick, M. (2005b) Melting and melt segregation in the aureole of the Glenmore Plug, Ardnamurchan. Journal of Metamorphic Geology 23: 29-43, 10.1111/j.1525-1314.2005.00560.x

Holness, M.B. & Graham, C.M. (1995) P-T-X effects on equilibrium carbonate-H_2O-CO_2-NaCl dihedral angles: constraints on carbonate permeability and the role of deformation during fluid infiltration. Contributions to Mineralogy and Petrology 119: 301-313, 10.1007/BF00307289

Holness, M.B., Hallworth, M. A., Woods, A. & Sides, R.E. (2007b) Partial melting and metasomatism of cumulates by intrusive magma replenishment: the Wavy Horizon, Isle of Rum, Scotland. Journal of Petrology 48: 563-587, 10.1093/petrology/egl072

Holness, M.B. & Humphreys, M.C.S. (2003) The Traigh Bhén na Sgùrra sill, Isle of Mull: flow localization in a major magma conduit. Journal of Petrology 44: 1961-1976, 10.1093/petrology/egg066

Holness, M.B., Martin, V.M. & Pyle, D.M. (2005c) Information about open-system magma chambers derived from textures in magmatic enclaves: the Kameni Islands, Santorini, Greece. Geological Magazine 142: 637-649, 10.1017/S0016756805001172

Holness, M.B., Morse, S.A. & Tegner, C. (2009) Response to Comment by McBirney, Boudreau and Marsh. Journal of Petrology 50: 97-102, 10.1093/petrology/egn074

Holness, M.B. & Sawyer, E.W. (2008) On the pseudomorphing of melt-filled pores in migmatites. Journal of Petrology 49: 1343-1363, 10.1093/petrology/egn028

Holness, M.B., Tegner, C., Nielsen, T.F.D., Stripp, G. & Morse, S.A. (2007a) A textural record of solidification and cooling in the Skaergaard intrusion, East Greenland. Journal of Petrology 48: 2359-2377, 10.1093/petrology/egm064

Holness, M.B. & Winpenny, B. (2009) The Unit 12 allivalite, Eastern Layered Intrusion, Isle of Rum: a textural and geochemical study of an open-system magma chamber. Geological Magazine 146: 437-450, 10.1017/S0016756808005797

Holzeid, A., Schmitz, M.D. & Grove, T.L. (2000) Textural equilibria of iron sulfide liquids in partially molten silicate aggregates and their relevance to core formation scenarios. Journal of Geophyscial Research 105: 13555-13567, 10.1029/2000JB900046

Hunter, R.H. (1987) Textural equilibrium in layered igneous rocks. In: (ed. Parsons, I.) Origins of igneous layering. Dordrecht: D. Reidel. pp. 473-503.

Hunter, R.H. (1996) Texture development in cumulate rocks. In: (ed. Cawthorn, R.G.) Layered Intrusions. Developments in Petrology 15: 77-101. Elsevier Science B.V.

Hunter, R.H. & McKenzie, D. (1989) The equilibrium geometry of carbonatite melts in rocks of mantle composition. Earth and Planetary Science Letters 92: 347-356, 10.1016/0012-821X(89)90059-9

Ikeda, S., Toriumi, M., Yoshida, H. & Shimizu, I. (2002) Experimental study of the textural development of igneous rocks in the late stage of crystallization: the importance of interfcial energies under non-equilibrium conditions. Contributions to Mineralogy and Petrology 142: 397-415, 10.1007/s004100100300

Jin, Z.-M., Green, H.W. & Zhou, Y. (1993) Melt topology in partially molten mantle peridotite during ductile deformation. Nature 372: 164-167, 10.1038/372164a0

Jurewicz, S.R. & Jurewicz, A.J.G. (1986) Distribution of apparent angles on random sections, with emphasis on dihedral angle measurements. Journal of Geophysical Research 91: 9277-9282, 10.1029/JB091iB09p09277

Jurewicz, S.R. & Watson, E.B. (1984) Distribution of partial melt in a felsic system: the importance of surface energy. Contributions to Mineralogy and Petrology 85: 25-29, 10.1007/BF00380218

Jurewicz, S.R. & Watson, E.B. (1985) The distribution of partial melt in a granitic system: the application of liquid phase sintering theory. Geochimica et Cosmochimica Acta 49: 1109-1121, 10.1016/0016-7037(85)90002-X

Kile, D.E. (2009) The Universal Stage: the past, present and future of a mineralogical research instrument. http://www.geochemsoc.org/publications/geochemicalnews/gn140jul09/theuniversalstage.htm

Kostenko, O., Jamtveit, B., Austrheim, H., Pollok, K. & Putnis, C. (2002) The mechanism of fluid infiltration in peridotites at Almklovdalen, western Norway. Geofluids 2: 203-215, 10.1046/j.1468-8123.2002.00038.x

Kretz, R. (1966) Interpretation of the shape of mineral grains in metamorphic rocks. Journal of Petrology 7: 68-94.

Kruhl, J.H. (2001) Crystallographic control on the development of foam textures in quartz, plagioclase and analogue material. International Journal of Earth Sciences (Geologisches Rundschau) 90: 104-117, 10.1007/s005310000170

Kruhl, J.H. & Peternell, M. (2002) The equilibration of high-angle grain boundaries in dynamically recrystallized quartz: the effect of crystallography and temperature. Journal of Structural Geology 24: 1125-1137, 10.1016/S0191-8141(01)00096-7

Laporte, D. (1994) Wetting behaviour of partial melts during crustal anatexis: the distribution of hydrous silicic melts in polycrystalline aggregates of quartz. Contributions to Mineralogy and Petrology 116: 486-499, 10.1007/BF00310914

Laporte, D. & Provost, A. (2000) Equilibrium geometry of a fluid phase in a polycrystalline aggregate with anisotropic surface energies: Dry grain boundaries. Journal of Geophysical Research 105: 25937-25953, 10.1029/2000JB900256

Laporte, D. & Watson, E.B. (1995) Experimental and theoretical constraints on the melt distribution in crustal sources: the effect of crystalline anisotropy on melt interonnectivity. Chemical Geology 124: 161-184, 10.1016/0009-2541(95)00052-N

Leibl, C., Kuntcheva, B., Kruhl, J.H. & Kunze, K. (2007) Crystallographic orientations of quartz grain-boundary segments formed during dynamic recrystallisation and subsequent annealing. European Journal of Mineralogy 19: 735-744, 10.1127/0935-1221/2007/0019-1759

Longhi, J. & Jurewicz, S.R. (1995) Plagioclase-melt wetting angles and textures: implications for anorthosites. Lunar and Planetary Science XXVI: 859-860.

Lupulescu, A. & Watson, E.B. (1999) Low melt fraction connectivity of granitic and tonalitic melts in a mafic crustal rock at 800°C and 1 GPa. Contributions to Mineralogy and Petrology 134: 202-216. 10.1007/s004100050479

Lusk, J., Calder, B.O.E. & Freeman, T.E. (2002) Temperatures from triple-junction angles in sulfides. American Mineralogist 87:1390-1400.

Mader, H.M. (1992) Observations of the water-vein system in polycrystalline ice. Journal of Glaciology 38: 333-347.

Mann, U., Frost, D.J. & Rubie, D.C. (2008) The wetting ability of Si-bearing liquid Fe-alloys in a solid silicate matrix - percolation during core formation under reducing conditions? Physics of the Earth and Planetary Interiors 167: 1-7, 10.1016/j.pepi.2007.12.002

Martin, V.M., Holness, M.B. & Pyle, D.M. (2006) Textural analysis of magmatic enclaves from the Kameni Islands, Santorini, Greece. Journal of Volcanology and Geothermal Research 154: 89-102, 10.1016/j.jvolgeores.2005.09.021

Maumus, J., Laporte, D. & Schiano, P. (2004) Dihedral angle measurements and infiltration property of SiO 2-rich melts in mantle peridotite assemblages. Contributions to Mineralogy and Petrology 148: 1-12, 10.1007/s00410-004-0595-x

Mehnert, K.R., Büsch, W. & Schneider, G. (1973) Initial melting at grain boundaries of quartz and feldspar in gneisses and granulites. Neues Jahrbuch für Mineralogie, Monatschefte 4: 165-183.

Melia, T.P. & Moffitt, W.P. (1964) Crystallisation from aqueous solution. Journal of Colloid Science 19: 433-447, 10.1016/0095-8522(64)90043-1

Minarik, W.G., Ryerson, .FJ. & Watson, E.B. (1996) Textural entrapment of core-forming melts. Science 272: 530-533, 10.1126/science.272.5261.530

Minarik, W.G. & Watson, E.B. (1995) Interconnectivity of carbonate melt at low melt fraction. Earth and Planetary Science Letters 133: 350-357, 10.1016/0012-821X(95)00085-Q

Park, H.-H. & Yoon, D.N. (1985) Effect of dihedral angle on the morphology of grains in a matrix phase. Metallurgical transactions 16A: 923-928.

Parsons, R.A., Nimmo, F., Hustoft, J.W., Holtzman, B.K. & Kohlstedt, D.L. (2008) An experimental and numerical study of surface tension-driven melt flow. Earth and Planetary Science Letters 267: 548-557, 10.1016/j.epsl.2007.11.064

Pervukhina, M. & Kuwahara, Y. (2008) Correlations between electrical and elastic properties of solid-liquid composites with interfacial energy-controlled equilibrium microstructures. Earth and Planetary Science Letters 265: 410-422, 10.1016/j.epsl.2007.10.038

Pharr, G.M. & Ashby, M.F. (1983) On creep enhanced by a liquid phase. Acta Metallurgica 31: 129-138, 10.1016/0001-6160(83)90072-X

Platten, I. M. (1981) Partial melting of feldspathic quartzite around late Caledonian minor intrusions in Appin, Scotland. Geological Magazine 119: 413-419, 10.1017/S0016756800026327

Price, J.D., Wark, D.A., Watson, E.B. & Smith, A.M. (2006) Grain-scale permeability of faceted polycrystalline aggregates. Geofluids 6: 302-318, 10.1111/j.1468-8123.2006.00149.x

Putnis, A. & Mauthe, G. (2001) The effect of pore size on cementation in porous rocks. Geofluids 1: 37-41, 10.1046/j.1468-8123.2001.11001.x

Riegger, O.K. & Van Vlack, L.H.W. (1960) Dihedral angle measurement. Transactions of the Metallurgical Society of the AIME 218: 933-935.

Rose, L.A. & Brenan, J.M. (2001) Wetting properties of Fe-Ni-Co-Cu-O-S melts against olivine: implications for sulfide melt mobility. Economic Geology 96: 145-157, 10.2113/96.1.145

Sawyer, E.W. (1999) Criteria for the recognition of partial melting. Physics and Chemistry of the Earth 24: 269-279, 10.1016/S1464-1895(99)00029-0

Sawyer, E.W. (2001) Melt segregation in the continental crust: distribution and movement of melt in anatectic rocks. Journal of Metamorphic Geology 19: 291-309, 10.1046/j.0263-4929.2000.00312.x

Schafer, F.N. & Foley, S.F. (2002) The effect of crystal orientation on the wetting behaviour of silicate melts on the surfaces of spinel peridotite minerals. Contributions to Mineralogy and Petrology 143: 254-261, 10.1007/s00410-001-0339-0

Schenk, O. & Urai, J.L. (2004) Microstructural evolution and grain boundary structure during static recrystallisation in synthetic polycrystals of sodium chloride containing saturated brine. Contributions to Mineralogy and Petrology 146: 671-682, 10.1007/s00410-003-0522-6

Scherer, G.W. (1999) Crystallisation in pores. Cement and Concrete Research 29: 1347-1358, 10.1016/S0008-8846(99)00002-2

Shannon, M.C. & Agee, C.B. (1996) High pressure constraints on percolative core formation. Geophysical Research Letters 23: 2717-2720, 10.1029/96GL02817

Sides, R. (2008) Crystal mushes in mafic magma chambers. Unpublished PhD thesis, University of Cambridge.

Smith, C.S. (1948) Grains, phases and interfaces: an interpretation of microstructure. Transactions of the Metallurgical Society of the AIME 175: 15-51.

Smith, C.S. (1964) Some elementary principles of polycrystalline microstructure. Metallurgical Reviews 9: 1-48.

Spetzler, H. & Anderson, D.L. (1968) The effect of temperature and partial melting on velocity and attenuation in a simple binary system. Journal of Geophysical Research 73: 6051-6060, 10.1029/JB073i018p06051

Stanton, R.L. (1964) Textures of stratiform ores. Nature 202: 173-174, 10.1038/202173a0

Stanton, R.L. & Gorman, H.A. (1968) A phenomenological study of grain boundary migration in some common sulfides. Economic Geology 63: 907-923, 10.2113/gsecongeo.63.8.907

Stickels, C.A. & Hücke, E.E. (1964) Measurement of dihedral angles. Transactions of the Metallurgical Society of AIME 230: 795-801.

Sutton, A.P. & Baluffi, R.W. (1996) Interfaces in crystalline materials. Monograph Physics and Chemistry of Materials 51. Clarendon, Oxford.

Takafuji, N., Hirose, K., Ono, S., Xu, F., Mitome, M. & Bando, Y. (2004) Segregation of core melts by permeable flow in the lower mantle. Earth and Planetary Science Letters 224: 249-257, 10.1016/j.epsl.2004.05.016

Takei, Y. (2000) Acoustic properties of partially molten media studied on a simple binary system with a controllable dihedral angle. Journal of Geophysical Research 105: 16665-16682, 10.1029/2000JB900124

Takei, Y. & Shimizu, I. (2003) The effects of liquid composition, temperature and pressure on the equilibrium dihedral angles of binary solid-liquid systems inferred from a lattice-like model. Physics of the Earth and Planetary Interiors 139: 225-242, 10.1016/j.pepi.2003.08.004

Terasaki, H., Frost, D.J., Rubie, D.C. & Langenhorst, F. (2005) The effect of oxygen and sulphur on the dihedral angle between Fe-O-S melt and silicate minerals at high pressure: implications for Martian core formation. Earth and Planetary Science Letters 232: 379-392, 10.1016/j.epsl.2005.01.030

Terasaki, H., Frost, D.J., Rubie, D.C. & Langenhorst, F. (2007) Interconnectivity of Fe-O-S liquid in polycrystalline silicate perovskite at lower mantle conditions. Physics of the Earth and Planetary Interiors 161: 170-176, 10.1016/j.pepi.2007.01.011

Terasaki, H., Frost, D.J., Rubie, D.C. & Langenhorst, F. (2008) Percolative core formation in planetesimals. Earth and Planetary Science Letters 237: 132-137, 10.1016/j.epsl.2008.06.019

Toramaru, A . & Fujii, N. (1986) Connectivity of melt phase in a partially molten peridotite. Journal of Geophysical Research 91: 9239-9252, 10.1029/JB091iB09p09239

Vernon, R.H. (1968) Microstructures of high-grade metamorphic rocks at Broken Hill, Australia. Journal of Petrology 9: 1-22.

Vernon, R.H. (1970) Comparative grain-boundary studies of some basic and ultrabasic granulites, nodules and cumulates. Scottish Journal of Geology 6: 337-351, 10.1144/sjg06040337

Vernon, R.H. (1997) Comment: On the identification of textural disequilibrium in rocks using dihedral angle measurements. By Elliott, M.T. & Cheadle, M.J. Geology 25: 1055, 10.1130/0091-7613(1997)025<1055:OTIOTD>2.3.CO;2

Vernon, R.H. (2004) A practical guide to rock microstructure. Cambridge University Press, Cambridge UK. pp 579.

Voll, G. (1960) New work on petrofabrics. Liverpool and Manchester Geological Journal 2: 503-567.

Voll, G. (1969) Klastische Mineralien aus den Sedimentserien der Schottischen Highlands und ihr Schicksal bei aufsteigender Regional- und Kontaktmetamorphose. Habilitationsschrift, Fakultät für Bergbau und Hüttenwesen, Technische Universität Berlin, D83.

Von Bargen, N. & Waff, H.S. (1986) Permeabilites, interfacial areas and curvatures of partially molten systems: results of numerical computations of equilibrium microstructures. Journal of Geophysical Research 91: 9261-9276, 10.1029/JB091iB09p09261

Von Bargen, N. & Waff, H.S. (1988) Wetting of enstatite by basaltic melt at 1350˚C and 1.0 to 2.5 GPa pressure. Journal of Geophysical Research 93: 1153-1158. 10.1029/JB093iB02p01153

Waff, H.S. & Bulau, J.R. (1979) Equilibrium fluid distribution in an ultramafic partial melt under hydrostatic stress conditions. Journal of Geophysical Research 84: 6109-6114, 10.1029/JB084iB11p06109

Waff, H.S. & Faul, U.H. (1992) Effects of crystalline anisotropy on fluid distribution in ultramafic partial melts. Journal of Geophysical Research 97: 9003-9014, 10.1029/92JB00066

Wager, L.R., Brown, G.M. & Wadsworth, W.J. (1960) Types of igneous cumulates. Journal of Petrology 1: 73-85.

Walford, M.E.R. & Nye, J.F. (1991) Measuring the dihedral angle of water at a grain boundary in ice by an optical diffraction method. Journal of Glaciology 37: 107-112.

Walker, D., Jurewicz, S. & Watson, E.M. (1988) Adcumulus dunite growth in a laboratory thermal gradient. Contributions to Mineralogy and Petrology 99: 306-319, 10.1007/BF00375364

Watson, E.B., Brenan, J.M. & Baker, D.R. (1990) Distribution of fluids in the continental mantle. In: Continental Mantle (ed. Menzie MA). Monographs on Geology and Geophysics 16: 111-125.

Wray, P.J. (1976) The geometry of two-phase aggregates in which the shape of the second phase is determined by its dihedral angle. Acta Metallurgica 24: 125-135, 10.1016/0001-6160(76)90015-8

Yoshino, T., Matsuzaki, T., Shatskiy, A. & Katsura, T. (2009) The effect of water on the electrical conductivity of olivine aggregates and its implications for the electrical structure of the upper mantle. Earth and Planetary Science Letters 288: 291-300, 10.1016/j.epsl.2009.09.032

Yoshino, T., Mibe, K., Yasuda, A. & Fujii, T. (2002) Wetting properties of anorthite aggregates; implications for fluid connectivity in continental lower crust. Journal of Geophysical Research 107: 10.1029/2001JB000440. ECV 10.1-8

Yoshino, T., Nishihara, Y. & Karato, S.-I. (2007) Complete wetting of olivine grain boundaries by a hydrous melt near the mantle transition zone. Earth and Planetary Science Letters 256: 466-472, 10.1016/j.epsl.2007.02.002

Yoshino, T., Price, J.D., Wark, D.A. & Watson, E.B. (2006) Effect of faceting on pore geometry in texturally equilibrated rocks: implications for low permeability at low porosity. Contributions to Mineralogy and Petrology 152: 169-186, 10.1007/s00410-006-0099-y

Yoshino, T., Takei, Y., Wark, D.A. & Watson, E.B. (2005) Grain boundary wetness of texturally equilibrated rocks, with implications for seismic properties of the upper mantle. Journal of Geophysical Research 110: B08205, 10.1029/2004JB003544